Rung-Arunwan *et al. Earth, Planets and Space* (2017) 69:80
DOI 10.1186/s40623-017-0665-8

Earth, Planets and Space

FULL PAPER

Open Access

Use of ssq rotational invariant of magnetotelluric impedances for estimating informative properties for galvanic distortion

T. Rung-Arunwan[1,2,3,4*], W. Siripunvaraporn[1,2] and H. Utada[3]

Abstract

Several useful properties and parameters—a model of the regional mean one-dimensional (1D) conductivity profile, local and regional distortion indicators, and apparent gains—were defined in our recent paper using two rotational invariants (det: determinant and ssq: sum of squared elements) from a set of magnetotelluric (MT) data obtained by an array of observation sites. In this paper, we demonstrate their characteristics and benefits through synthetic examples using 1D and three-dimensional (3D) models. First, a model of the regional mean 1D conductivity profile is obtained using the average ssq impedance with different levels of galvanic distortion. In contrast to the Berdichevsky average using the average det impedance, the average ssq impedance is shown to yield a reliable estimate of the model of the regional mean 1D conductivity profile, even when severe galvanic distortion is contained in the data. Second, the local and regional distortion indicators were found to indicate the galvanic distortion as expressed by the splitting and shear parameters and to quantify their strengths in individual MT data and in the dataset as a whole. Third, the apparent gain was also shown to be a good approximation of the site gain, which is generally claimed to be undeterminable without external information. The model of the regional mean 1D profile could be used as an initial or a priori model in higher-dimensional inversions. The local and regional distortion indicators and apparent gains could be used to examine the existence and to guess the strength of the galvanic distortion. Although these conclusions were derived from synthetic tests using the Groom–Bailey distortion model, additional tests with different distortion models indicated that these conclusions are not strongly dependent on the choice of distortion model. These galvanic-distortion-related parameters would also assist in judging if a proper treatment is needed for the galvanic distortion when an MT dataset is given. Hence, this information derived from the dataset would be useful in MT data analysis and inversion.

Keywords: Magnetotellurics, Rotational invariant, Galvanic distortion

Introduction

To obtain reliable three-dimensional (3D) inversion from magnetotelluric (MT) data, either distorted or undistorted, the choice of an initial or a priori model is crucial. The benefit of having a good model of the regional mean one-dimensional (1D) profile as an initial or a priori model has been reported in previous studies. For example, the optimal model of the mean 1D conductivity profile would minimize the lateral conductivity contrast, which could yield a better-conditioned system of equations (Avdeev 2005). Furthermore, the use of the mean 1D profile as an a priori model would result in the rapid and stable convergence of higher-dimensional inversion problems (Tada et al. 2012).

If no other independent information is available, the initial model can be constructed from the mean 1D conductivity profile, which will be described in the following. Ideally, if we had a sufficiently large number of electromagnetic (EM) observation sites densely distributed over the globe, the global mean conductivity profile could

*Correspondence: t.rungarunwan@gmail.com
[1] Department of Physics, Faculty of Science, Mahidol University, 272 Rama 6 Road, Rachatawee, Bangkok 10400, Thailand
Full list of author information is available at the end of the article

be defined as the azimuthal average of the conductivity along a variable depth:

$$\sigma_0(z) = \frac{1}{S_0(z)} \oiint \sigma(z,\theta,\phi)\mathrm{d}S, \tag{1}$$

where $\sigma(z,\theta,\phi)$ is the distribution of the Earth's electrical conductivity, $S_0(z)$ is the total surface area of the Earth at depth z, and $\mathrm{d}S$ is a spherical surface element. Once the global mean 1D conductivity profile is obtained in this way (Eq. 1), the 3D conductivity distribution at any position within the Earth can be expressed as a combination of the global mean 1D model and the azimuthal conductivity contrast as

$$\sigma(z,\theta,\phi) = \sigma_0(z) + \Delta\sigma(z,\theta,\phi). \tag{2}$$

The definition of the global mean 1D conductivity profile and the azimuthal contrast is clear in theory, but the estimation of them is not easy in practice. Although it is possible to perform global induction studies using geomagnetic observatory data, there are significant differences among existing inverted models (e.g., Kelbert et al. 2009; Kuvshinov and Semenov 2012; Semenov and Kuvshinov 2012). Most likely, such attempts may include biases due to the nonuniformity of their site distributions or false images resulting from spatial aliasing (Utada and Munekane 2000) because the distributions of existing geomagnetic observatories and MT observation sites are spatially nonuniform. More importantly, the EM induction method is generally sensitive to the conductivity beneath each observation site.

Practically, EM exploration, e.g., MT survey, focuses on a limited region where numerous observations are made. In this study, we consider a case in which the corresponding induction scale length is much smaller than the radius of the Earth; hence, the sphericity of the Earth can be ignored. Such a case is usually called a regional or local induction study. From a given array of observations, the following regional mean 1D conductivity profile $\sigma_\mathrm{R}(z)$ can be obtained from the areal average of the conductivity:

$$\sigma_\mathrm{R}(z) = \frac{1}{A_0} \iint \sigma(x,y,z)\,\mathrm{d}A \tag{3}$$

where A_0 is the arbitrary area in which the observation sites are distributed, $\mathrm{d}A$ is a surface element, and $\sigma(x,y,z)$ is the regional 3D conductivity distribution. Alternatively, we may use the logarithmic average to define the regional mean 1D profile:

$$\log\sigma_\mathrm{R}(z) = \frac{1}{A_0} \iint \log\sigma(x,y,z)\,\mathrm{d}A. \tag{4}$$

Mathematically, the logarithmic scale average of the conductivity gives less conductive structure. As with Eq. (2), the regional conductivity distribution can be expressed as a combination of the regional mean 1D profile and the conductivity contrast $\Delta\sigma(x,y,z)$:

$$\sigma(x,y,z) = \sigma_\mathrm{R}(z) + \Delta\sigma(x,y,z). \tag{5}$$

When the regional mean 1D conductivity profile is written as the areal average (Eqs. 3 or 4) of the conductivity from any 3D conductivity distribution, deviations in the conductivity higher or lower than the average value are regarded as conductivity anomalies of positive or negative contrast, respectively. $\sigma_\mathrm{R}(z)$ defined either by Eqs. (3) or (4) is also regarded as an optimal mean 1D conductivity profile in the sense that the variance of $\Delta\sigma(x,y,z)$ is minimized (Rung-Arunwan et al. 2016).

The regional mean 1D profile $\sigma_\mathrm{R}(z)$ is practically unknown beforehand, although it can be estimated from $\sigma(x,y,z)$ inverted from the observed data. However, in this study, we use an alternate method in which $\sigma_\mathrm{R}(z)$ is first estimated from the observed data in the area of interest. The conductivity model, either $\sigma(x,y,z)$ or $\Delta\sigma(x,y,z)$, can then be estimated by 3D inversion using $\sigma_\mathrm{R}(z)$ as a priori information or a starting model.

This poses the problem of how to reliably estimate a model of the regional mean 1D profile from an array of MT observations in a general 3D situation. Baba et al. (2010) already presented a solution to such a problem in the case of a seafloor MT study. Here, we consider the case in which MT data are obtained from an array of observations on land. The solution of this problem is not straightforward because MT data on land are usually affected by galvanic distortion, i.e., an alteration in the MT impedance due to near-surface small-scale heterogeneity that is smaller than a typical site spacing and confined to be shallower than the inductive scale length of interest (Ledo et al. 1998; Utada and Munekane 2000; Bibby et al. 2005). In other words, the physical dimensions of the distorting bodies are smaller than their inductive scale length and also that of the host.

Berdichevsky et al. (1980) proposed a scheme to estimate a model of the mean 1D profile from distorted data by averaging the effective resistivity, which is equivalent to the apparent resistivity derived from the determinant of the impedance tensor (hereafter denoted as the det impedance, $Z_\mathrm{det} = \sqrt{Z_{xx}Z_{yy} - Z_{xy}Z_{yx}}$). This is a statistical approach to smooth the effect of galvanic distortion that is supposed to be a random phenomenon, and the average in this method is referred to as the Berdichevsky average (Rung-Arunwan et al. 2016). When it was first introduced, the det impedance was generally used in regional studies (e.g., Berdichevsky et al. 1980; Jones 1988; Berdichevsky et al. 1989). However, it was later adopted in two-dimensional (2D) MT applications (e.g., Oldenburg and Ellis 1993; Pedersen and Engels

2005). It is also applied as the current channeling indicator (Lezaeta and Haak 2003) and used in environmental applications (Falgàs et al. 2009). The det impedance has also been used in recent works. For example, Seama et al. (2007) inverted the det impedances from marine MT data at each observation point to obtain 1D conductivity profiles beneath the Philippine Sea, Arango et al. (2009) used the det impedance to interpret 3D MT data, and Baba et al. (2010) and Avdeeva et al. (2015) used the average det impedance in the same way as Berdichevsky et al. (1980).

However, when the det impedance was re-examined on the basis of the present knowledge of galvanic distortion by applying the Groom–Bailey model (Groom and Bailey 1989), it was found that the magnitude of the det impedance is always biased downward by the geometric distortion expressed by the shear and splitting parameters (see Gómez-Treviño et al. 2013; Rung-Arunwan et al. 2016). Note that Gómez-Treviño et al. (2013) studied the effect of galvanic distortion on the rotational invariants in the case of 2D regional structures. Even in the absence of a site gain, the Berdichevsky average causes downward bias in the apparent resistivity as compared with those from the regional mean 1D conductivity profile ($\sigma_{\mathrm{R}}(z)$) defined by Eqs. (3) or (4) (Rung-Arunwan et al. 2016).

Rung-Arunwan et al. (2016) proposed another method for estimating the model of the mean 1D profile that was similar to the method of using the Berdichevsky average but redefined it with another rotational invariant: the sum of the squared elements of the impedance tensor (ssq impedance) $Z_{\mathrm{ssq}} = \sqrt{\left(Z_{xx}^2 + Z_{xy}^2 + Z_{yx}^2 + Z_{yy}^2\right)/2}$ (Szarka and Menvielle 1997). Note that the ssq and det impedances are identical in the case of 1D earth, but for 2D and 3D earth, the induction sensed by the ssq and det impedances is different (see also Szarka and Menvielle 1997) by $Z_{\mathrm{ssq}}^2 - Z_{\mathrm{det}}^2 = \frac{1}{2}(Z_{xx} - Z_{yy})^2 + \frac{1}{2}(Z_{xy} + Z_{yx})^2$. In comparison with the det impedance, the ssq impedance has been proven to be less biased by the distortion parameters (see Gómez-Treviño et al. 2013; Rung-Arunwan et al. 2016). An example of the field data from the western part of Thailand is shown in Fig. 1. The field example is consistent with the theoretical prediction presented in Rung-Arunwan et al. (2016) that the det impedance will have a smaller magnitude than the ssq impedance. According to the prediction, the downward bias for the det impedances is supposed to be caused by a geometric (shear and splitting) effect because the phase characteristics are almost identical. Consequently, the use of average ssq impedance is expected to more reliably estimate the model of the regional mean 1D profile than the use of the det impedance. Thus, this field example motivated us to present a systematic investigation of the approaches proposed by Rung-Arunwan et al. (2016) in this paper.

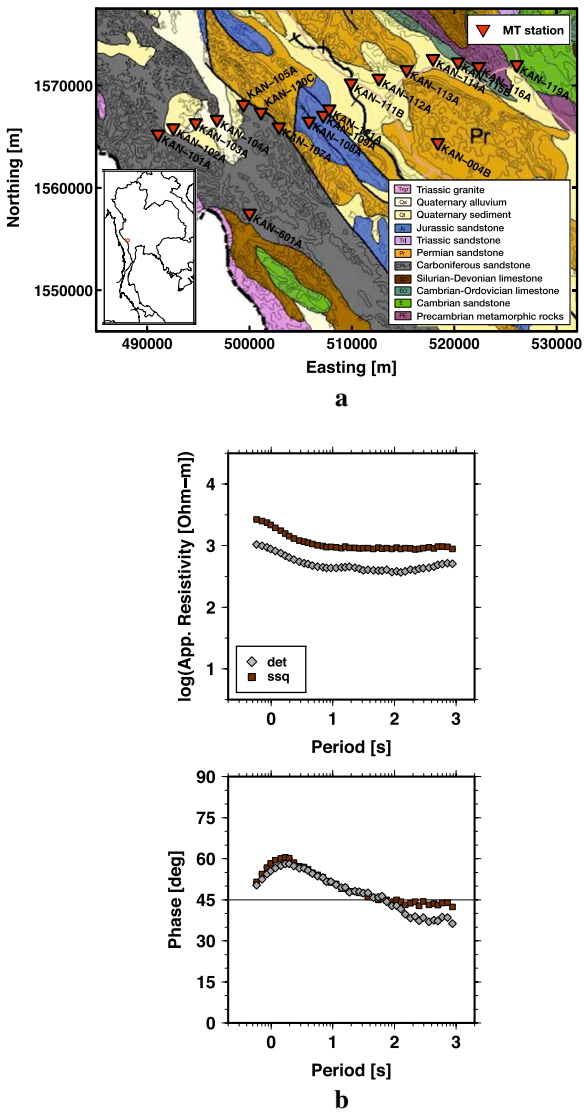

Fig. 1 **a** Map showing the cluster of 19 MT stations from the western part of Thailand (see Boonchaisuk et al. 2013). They are *plotted* on the geological map of this area (after Department of Mineral Resources 2006). **b** Example of rotational invariant, det (*gray diamonds*) and ssq (*brown squares*), impedances from an individual station (KAN-120C). The det impedances have magnitudes smaller than the ssq impedances, which is as predicted (Rung-Arunwan et al. 2016) because the det impedance is biased downward by geometric distortion

Identification and removal methods for galvanic distortion remain undetermined (Chp. 6 in Chave and Jones 2012), although several attempts to solve the problem of galvanic distortion have been presented. Some studies assumed a 2D Earth (e.g., Bahr 1988; Groom and Bailey 1989), whereas others confronted the nonuniqueness of

the obtained solution (e.g., Bibby et al. 2005). Moreover, Gómez-Treviño et al. (2014) presented an approach to estimate the 2D regional impedance and distortion parameters, i.e., twist and shear in the Groom–Bailey model, using the det and ssq impedances. Inversion based on the phase tensor (Caldwell et al. 2004), which yields a well-defined distortion-free solution, is also a promising strategy. However, the phase tensor is only a partial solution; thus, the inverted model strongly depends on the initial model (Patro et al. 2013; Tietze et al. 2015). In addition to decomposition approaches, inversion schemes that simultaneously solve the static shift (e.g., Sasaki and Meju 2006) have become feasible, but the geometric distortion is not controlled. Avdeeva et al. (2015) proposed 3D inversion with the solution of the full distortion matrix, but this approach does not allow this static shift to be a free parameter.

Although a number of approaches for handling galvanic distortion have been developed, an approach for determining the presence of galvanic distortion in the observed data has not been presented, except the concept of galvanic distortion indicators by Rung-Arunwan et al. (2016). The ability to identify the presence of galvanic distortion—either geometric or scaling—contained in the observed data and to quantify their intensity is undoubtedly important because the application of the galvanic distortion treatment to the observed data without knowing the presence of galvanic distortion and doing so may either improve or deteriorate the reliability of MT data interpretation.

Rung-Arunwan et al. (2016) proposed two types of galvanic distortion indicators. First, the local and regional distortion indicators are used to determine the strength of the geometric distortion as expressed by the shear and splitting effects on the basis of the fact that the geometric distortion (shear and splitting) has different effects on the det and ssq impedances. Second, the apparent gain is defined to be an approximation of the site gain (scaling in the impedance magnitude), which has been presumed to be indeterminable without other independent information (Groom et al. 1993; Bibby et al. 2005). These parameters may help quantitatively indicate the strength of the galvanic distortion posed in MT data. In addition, the employment of these two types of properties allows the effect of the site gain to be separated from the effects of the twist, shear, and splitting parameters. Most importantly, we can use these parameters to determine the necessary treatment of galvanic distortion for a given dataset, such as whether or not a removal scheme should be applied in the inversion (e.g., Sasaki and Meju 2006; Avdeeva et al. 2015).

The aim of this paper is to present synthetic examples for estimating a model of the regional mean 1D profile, the local and regional distortion indicators, and the apparent gains using the methods proposed by Rung-Arunwan et al. (2016). First, the proposed methods are briefly summarized. The results from 1D examples are then discussed to illustrate the basic concepts and the behavior of the proposed properties and parameters. In addition to the estimation of the model of the regional mean 1D profile from distorted sets of synthetic 3D impedances, the estimated model of the mean 1D profile is compared with $\sigma_{\mathrm{R}}(z)$ defined by Eqs. (3) or (4) for 3D examples. The numerical results of the local and regional distortion indicators and the apparent gains are presented and verified with synthetic values. In Rung-Arunwan et al. (2016) and this paper, the Groom–Bailey model of galvanic distortion is chosen, simply because the site gain is distinguished from the geometric distortion whose operators are normalized with their Frobenius norms. Still, the choice of galvanic distortion model may be arbitrary. Thus, numerical examples and a discussion regarding the galvanic distortion model dependence of the proposed methods are provided.

Theoretical background

This section briefly summarizes the method for estimating a model of the regional mean 1D profile and a set of parameters related to the galvanic distortion, which were presented in Rung-Arunwan et al. (2016).

First, a model of the regional mean 1D profile is estimated by inverting the average ssq impedances. As has been algebraically proven, the ssq impedance is relatively less sensitive to the effects of the shear and splitting parameters e and s, which are also called the geometric distortion, than the det impedance, the amplitude of which is always biased downward by these two parameters (Rung-Arunwan et al. 2016). After re-examination with the Groom–Bailey model of galvanic distortion, the Berdichevsky average is written as

$$\begin{aligned}\bar{Z}'_{\mathrm{det}}(\omega) &= \left[\prod_{i=1}^{N} Z'_{\mathrm{det}}(\mathbf{r}_i;\omega)\right]^{\frac{1}{N}} \\ &\approx \left[\prod_{i=1}^{N} \sqrt{\frac{(1-e_i^2)(1-s_i^2)}{(1+e_i^2)(1+s_i^2)}}\right]^{\frac{1}{N}} Z^{\mathrm{R}}_{\mathrm{det}}(\omega),\end{aligned} \tag{6}$$

where $Z'_{\mathrm{det}}(\mathbf{r}_i;\omega)$ is the det impedance of the ith observed (perhaps distorted) MT impedance at the position $\mathbf{r}_i$; e_i and s_i are the shear and splitting parameters at the ith station, respectively; N is the total number of observations; ω is the angular frequency; and $Z^{\mathrm{R}}_{\mathrm{det}}(\omega)$ is the regional det impedance. Note that the twist parameter has no effect on the det and ssq impedances (also discussed in Gómez-Treviño et al. 2013; Rung-Arunwan et al. 2016). If geometric distortion is contained in the data, the coefficient

in Eq. (6) becomes effective and is always smaller than unity. Hence, the use of the Berdichevsky average always gives a downward-biased regional 1D impedance, which yields an inverted model of the structure that is more conductive than the true structure.

On the contrary, the ssq impedance was proven to be less affected by geometric distortion (Gómez-Treviño et al. 2013; Rung-Arunwan et al. 2016). Therefore, averaging the ssq impedances from an array of MT observations gives a good approximation of the true regional response:

$$\bar{Z}'_{\mathrm{ssq}}(\omega) = \left[\prod_{i=1}^{N} Z'_{\mathrm{ssq}}(\mathbf{r}_i;\omega)\right]^{\frac{1}{N}} \approx Z^{\mathrm{R}}_{\mathrm{ssq}}(\omega), \tag{7}$$

where $Z'_{\mathrm{ssq}}(\mathbf{r}_i;\omega)$ is the ssq impedance of the observed MT impedance tensor at the position $\mathbf{r}_i$ and $Z^{\mathrm{R}}_{\mathrm{ssq}}(\omega)$ is the regional ssq impedance (Rung-Arunwan et al. 2016). A detailed discussion regarding the geometric and arithmetic averages of the MT impedances can be found in Section 1 of the Additional file 1. Moreover, the validity of the approximate equality in Eq. (7) will be examined in Section 2 of the Additional file 1.

Additionally, a set of parameters related to the galvanic distortion is defined as follows.

The *local distortion indicator* (LDI) indicates the strength of the shear and splitting parameters at a single station individually and is defined as the squared ratio of the ssq impedance to the det impedance:

$$\gamma_i(\omega) = \frac{Z'_{\mathrm{ssq}}(\mathbf{r}_i;\omega)^2}{Z'_{\mathrm{det}}(\mathbf{r}_i;\omega)^2} \approx \frac{(1+e_i^2)(1+s_i^2)}{(1-e_i^2)(1-s_i^2)} \frac{Z^{\mathrm{R}}_{\mathrm{ssq}}(\mathbf{r}_i;\omega)^2}{Z^{\mathrm{R}}_{\mathrm{det}}(\mathbf{r}_i;\omega)^2}. \tag{8}$$

Defined in this way, the LDI is intrinsically independent of the site gain. As the twist parameter has no effect on the det and ssq impedances, the presence of the twist effect cannot be ascertained from the LDI. Employing the fact that the shear and splitting distortion affects the det and ssq impedances differently (Gómez-Treviño et al. 2013; Rung-Arunwan et al. 2016), the LDI represents the effects of the shear and splitting parameters as a combination, which is unlike the decomposition approaches (e.g., Groom and Bailey 1989; McNeice and Jones 2001; Gómez-Treviño et al. 2014), where the distortion parameters, twist and shear in particular, are estimated.

The *regional distortion indicator* (RDI) also indicates the strength of the shear and splitting parameters but on a regional scale, i.e., it quantitatively indicates how strongly distorted the dataset is on average. It is defined as the geometric mean of the LDIs:

$$\gamma_{\mathrm{R}}(\omega) = \left[\prod_{i=1}^{N} \gamma_i(\omega)\right]^{\frac{1}{N}} \approx \left[\prod_{i=1}^{N} \frac{(1-e_i^2)(1-s_i^2)}{(1+e_i^2)(1+s_i^2)}\right]^{\frac{1}{N}} \frac{\bar{Z}^{\mathrm{R}}_{\mathrm{ssq}}(\omega)^2}{\bar{Z}^{\mathrm{R}}_{\mathrm{det}}(\omega)^2}, \tag{9}$$

where $\bar{Z}^{\mathrm{R}}_{\mathrm{ssq}}(\omega)^2$ and $\bar{Z}^{\mathrm{R}}_{\mathrm{det}}(\omega)^2$ are the averages of the regional ssq and det impedances, respectively.

The *apparent gain* is defined as the ratio of a rotational invariant at a given position to its regional average. As we are interested in two rotational invariants, the corresponding apparent det and ssq gains are derived as

$$g_i^{\mathrm{det}}(\omega) = \frac{Z'_{\mathrm{det}}(\mathbf{r}_i;\omega)}{\bar{Z}'_{\mathrm{det}}(\omega)} \approx g_i \sqrt{\frac{(1-e_i^2)(1-s_i^2)}{(1+e_i^2)(1+s_i^2)}} \tag{10}$$

and

$$g_i^{\mathrm{ssq}}(\omega) = \frac{Z'_{\mathrm{ssq}}(\mathbf{r}_i;\omega)}{\bar{Z}'_{\mathrm{ssq}}(\omega)} \approx g_i, \tag{11}$$

where g_i is the site gain for the ith observation site. Obviously, if the data are strongly distorted, the apparent det gain underestimates the site gain because of the shear and splitting parameters. Thus, the apparent ssq gain is expected to be the more accurate approximation of the site gain when the data are strongly distorted. In the following sections, the characteristic and behaviors of these parameters are synthetically examined.

Estimation of a model of the regional mean 1D profile

Rung-Arunwan et al. (2016) proposed a modification to the Berdichevsky average—the use of the average ssq impedance instead of the average det impedance—to avoid biasing from galvanic distortion. This section examines whether the proposed method can reliably estimate a model of the regional mean 1D profile from synthetically distorted data.

Here, we synthesize the Earth conductivity model by a combination of 1D structure and lateral heterogeneity, as given by Eq. 5. The 1D part is based on a reference model of the continental crust and upper mantle by Jones (1999) and has the main features of a resistive upper crust and a conductive lower crust (Fig. 2a). In this model, the upper crust extends from 3.5 to 14.8 km in depth, and the lower crust extends to a depth of 33.3 km. The corresponding 1D impedance (Fig. 2b) was obtained from the analytical solution, i.e., the recursive formulas in terms of coth functions, for the 1D MT problem (e.g., Chave and Jones 2012). Note that the complex impedance is generally represented as an apparent resistivity and phase. Here, the period range was selected to sense a structure existing between 10 and 100 km in depth. Therefore, any small structures confined in the near-surface layer of a few kilometers or less, which is shallower than the inductive scale length of present interest, are considered to be galvanic distorters (Utada and Munekane 2000). We further assume for simplicity that galvanic distorters have

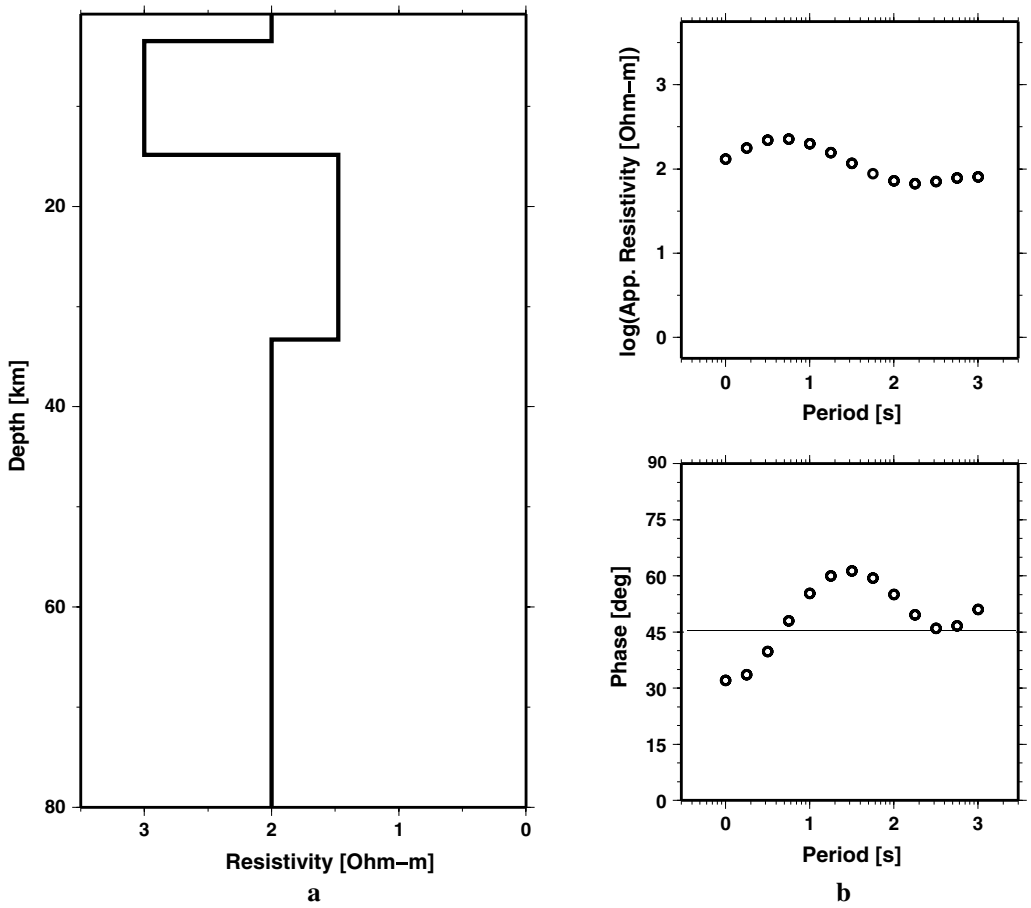

Fig. 2 **a** Layered-earth model used in this work. **b** Corresponding MT response (apparent resistivity and phase)

a typical size smaller than the typical site spacing of the observation array. The effect of these near-surface distorters is therefore a random phenomenon, and it can be expressed as a mathematical model such as the Groom–Bailey model of galvanic distortion, which is adopted in this work. The site gain and other distortion parameters (twist, shear, and splitting) are treated as random variables (e.g., Avdeeva et al. 2015).

The synthetic MT array contains 25 MT stations. Therefore, 25 cohorts of the site gain g and the twist t, shear e, and splitting s of the parameters of the Groom–Bailey model were generated following a normal distribution (Fig. 3). The distorted impedances were then calculated by applying these random parameter values to the synthetic impedances. More explicitly, we assumed that each set of distortion parameters has a mean of zero and is bounded by $(-1, +1)$. If any values are outside the bound, random numbers were generated again so that the set of random distortion parameters conforms with the bound. The random site gain was generated on a logarithmic scale without a bound. To quantitatively control the strength of the galvanic distortion, the standard deviation (SD) of the normal distribution of each parameter was varied. Five SD values of 0.1, 0.2, 0.3, 0.4, and 0.5 were used. Finally, five MT datasets with 25 stations each and different galvanic distortion strengths were considered.

1D example

First, we consider the simplest case with a 1D (horizontally stratified) Earth structure where the impedance at each site contains galvanic distortion. In this case, the galvanic distortion causes no phase mixing but only a static shift, g^2, which is the frequency-independent shift in the apparent resistivity (e.g., Beamish and Travassos 1992). As an example of distorted data, the ssq and det impedances from the synthetic 1D impedance distorted with $(g, t, e, s) = (1.20, 0.11, -0.37, 0.49)$ are shown in Fig. 4. Here, the synthetic site gain is greater than unity; therefore, the distorted ssq impedance is shifted upward. In general, the site gain equally affects the det and ssq impedances, i.e., the det impedance should also be shifted

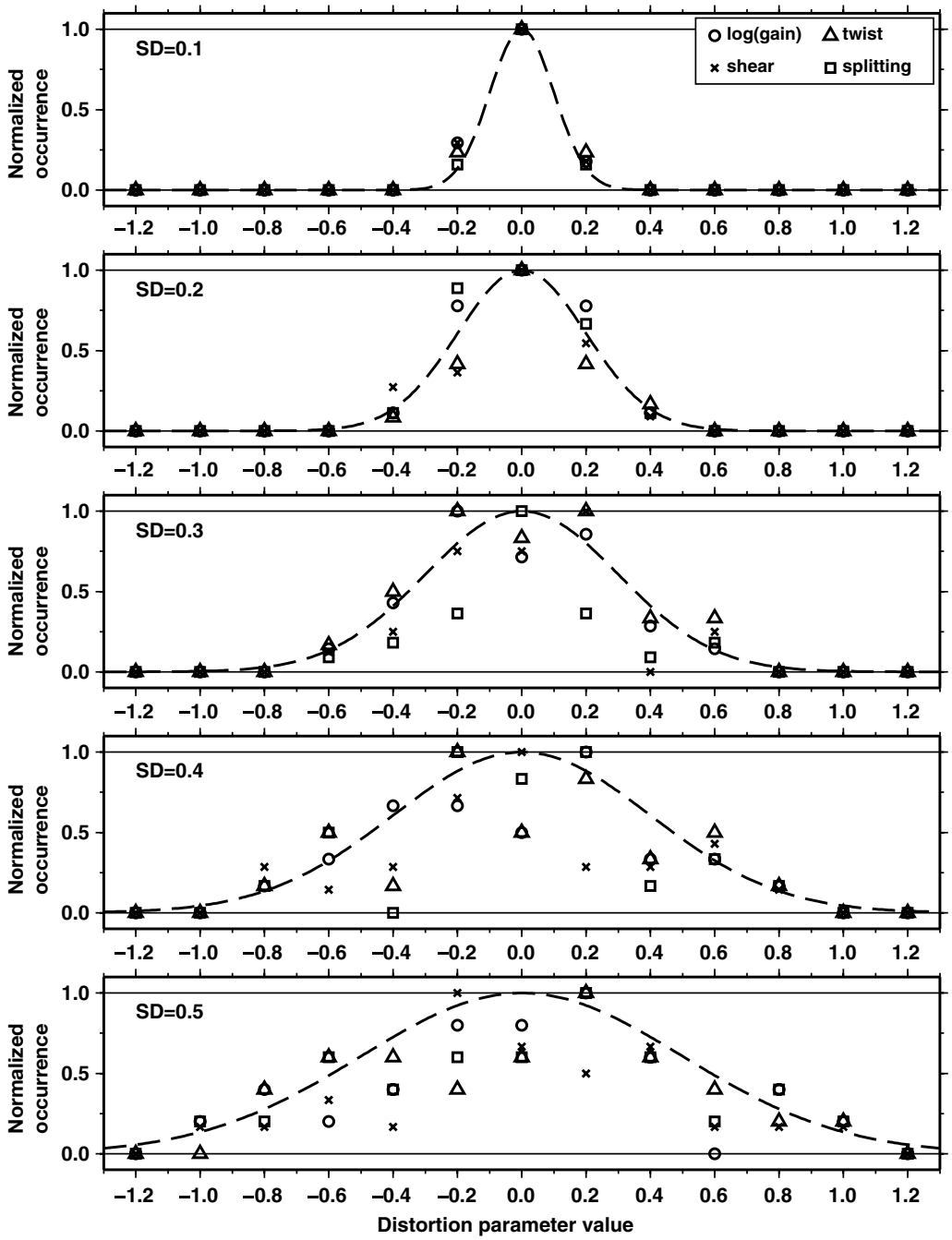

Fig. 3 Distributions of random distortion parameters with different SDs. The normalized occurrence is the number of occurrences divided by the maximum number of occurrences at a single parameter value. Each distribution is compared with the probability density function of the theoretical normal distribution for the given SD (*dashed lines*)

upward. However, the effect of the shear and splitting shifts the distorted det impedance downward instead. As a result, the magnitude of the distorted det impedance at this site is smaller than the undistorted one. All distorted sounding curves with an SD of 0.3 are shown in Fig. 5. These curves are shifted irregularly because of the random distortion parameters.

After the distortion parameters with different SDs were applied, five MT datasets with different galvanic distortion strengths were obtained. For each dataset, the average det and ssq impedances were then calculated using Eqs. (6) and (7) (Fig. 6), respectively. Here, the error bars indicate the SD, which were calculated in the logarithmic space, of the data and thus represent the level of

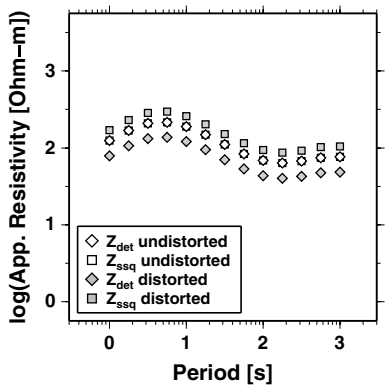

Fig. 4 Example of det (*diamonds*) and ssq (*squares*) impedances from the synthetic 1D impedance distorted with $(g, t, e, s) = (1.20, 0.11, -0.37, 0.49)$

dispersion in the galvanic distortion strengths. At equal distortion strengths, the distorted det impedances are generally more disperse than the ssq impedances, as demonstrated by the larger error bars in the det impedance results. This is a result of the fact that the det impedance is systematically biased downward by the shear and splitting parameters in addition to the effect of the site gain, whereas the ssq impedance is affected mostly by the site gain. The downward bias of the average det impedance becomes noticeable when the SD of the distortion parameters is greater than 0.2.

To obtain the regional mean 1D profile, the average invariant impedances were inverted with 1D Occam inversion, in which the second derivative of the conductivity with respect to the depth and conductivity is penalized (Constable et al. 1987). Here, the errors in the apparent resistivity and phase were fixed to 2.3% and 0.66°, respectively. All inverted models fit the data within a root-mean-square (RMS) misfit of unity. Because of the downward bias mentioned above, the models inverted from the average distorted det impedances tend to be more conductive than the synthetic profile when the distortion is stronger (Fig. 7a). As a consequence, the 1D models from the downward-biased det impedances may misinterpret the depth of the structure. Conversely, the average distorted ssq impedance is much less sensitive to the geometric distortion parameters; therefore, the models inverted from the distorted ssq impedances were all similar to that from the undistorted impedance (Fig. 7b). These numerical results confirmed the validity of the theoretical prediction that the average ssq impedance will yield an unbiased estimate of the regional 1D structure. Moreover, the behaviors of the det and ssq impedances under galvanic distortion, in which the det impedance is biased downward by and the ssq impedance is less sensitive to the geometric distortion, are also consistent with the numerical results presented in Gómez-Treviño et al. (2013). Next, we consider a case when the regional structure includes a 3D anomaly.

3D example

To generate synthetic 3D data, a model of a checkerboard structure with resistivities of 10 and 100 Ω m and a size of 80 km × 80 km each (Fig. 8) embedded in the lower crust of the layered-earth model used in the 1D example is constructed (Fig. 2a). The anomaly is large and systematic and corresponds to the inductive scale lengths (see Utada

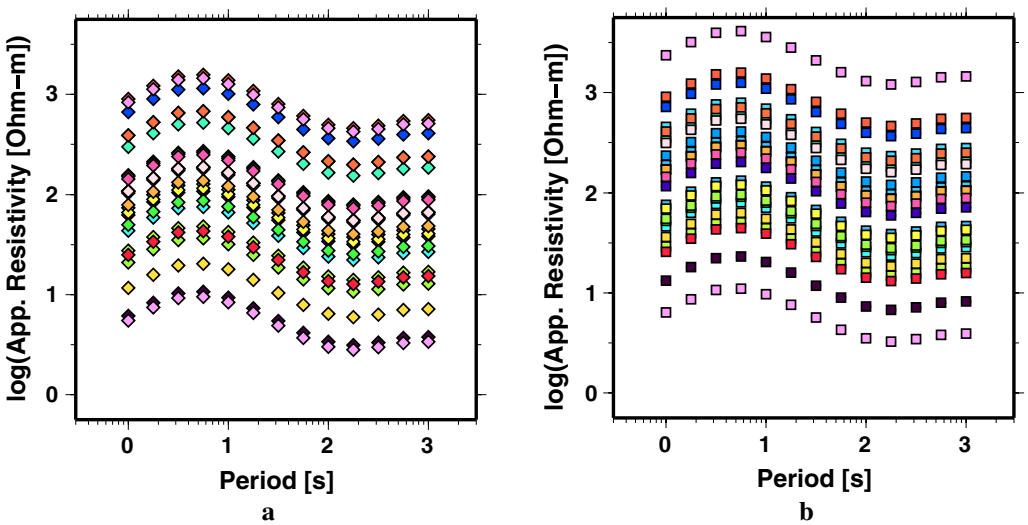

Fig. 5 Distorted **a** det and **b** ssq impedances from the 1D example, where a set of distortion parameters with an SD of 0.3 was applied. Each station is represented by a different *symbol color*

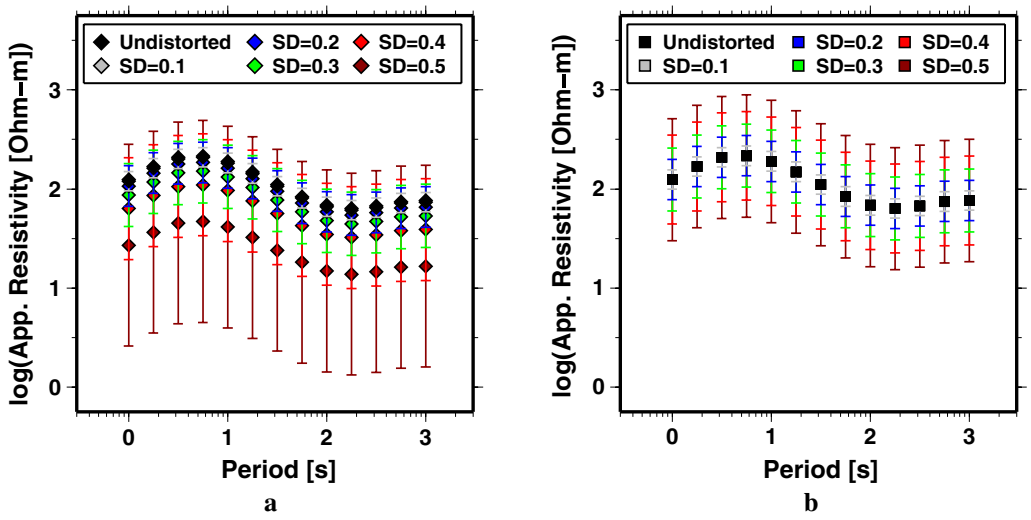

Fig. 6 Average **a** det and **b** ssq impedances from the 1D datasets distorted with different galvanic distortion strengths

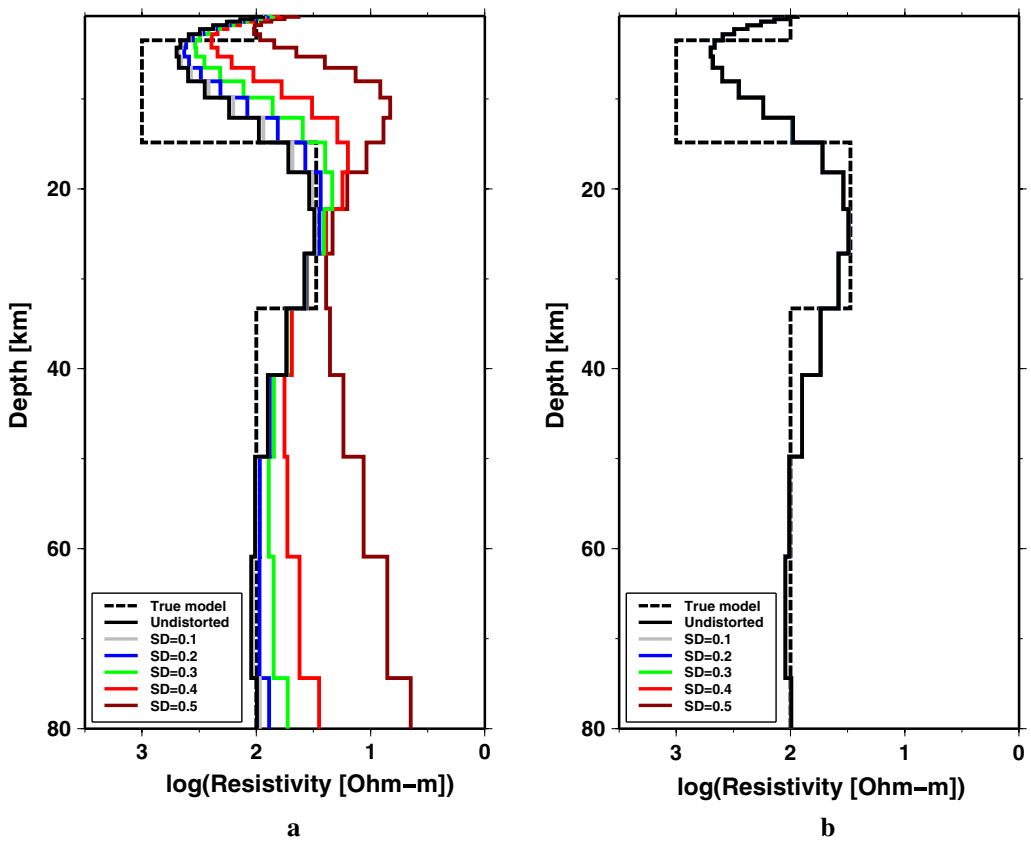

Fig. 7 1D models obtained by inverting the average **a** det and **b** ssq impedances from the distorted 1D datasets (Fig. 6). The synthetic profile is also shown as a *dashed line* for comparison. Note that all profiles are almost identical in (**b**)

and Munekane 2000) approximately ranging from 1.68 to 53.1 km at the shortest (1 s) and longest periods (1000 s), respectively. The inductive effect from the anomaly is expected to have a significant effect on the response because its corresponding inductive scale length is comparable to its physical dimension, and the 3D inductive effect from each anomaly is recognizable because it is embedded at a depth that could be recognized within the given period range. An array of 25 irregularly distributed MT stations was assumed to cover the 160 km × 160-km area of interest. The typical site spacing was then set to 32 km, which is smaller than the anomaly size. On average, each site represents an area of 32 km × 32 km (1/25 of the study area). The random location (x_i, y_i) of the ith station is given by

$$\begin{aligned} x_i &= x_c + s \times r_x \\ y_i &= y_c + s \times r_y, \end{aligned} \tag{12}$$

where (x_c, y_c) is the coordinate of the mesh center represented by each MT site; s is the typical site spacing, which is 32 km in this case; and r_x and r_y are uniform random numbers bounded by $(-0.5, +0.5)$.

In this work, the synthetic 3D MT responses were calculated using the software WSINV3DMT (Siripunvaraporn et al. 2005; Siripunvaraporn and Egbert 2009). The size of the entire checkboard anomaly is 320 km × 320 km, and the horizontal mesh resolution is 5.0 km × 5.0 km. The accuracy of the calculation with this resolution

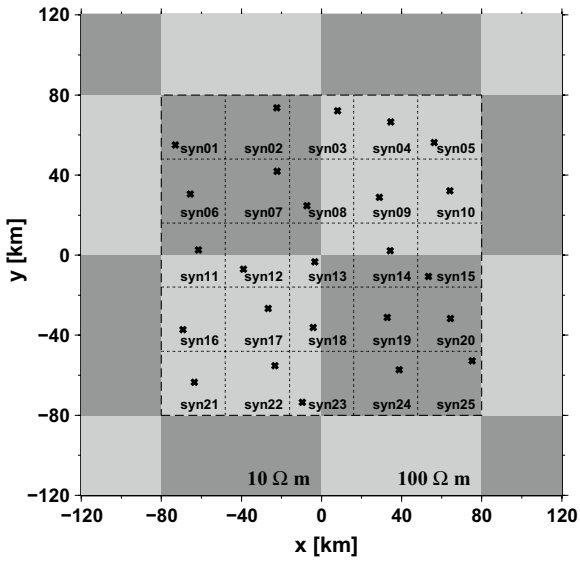

Fig. 8 Model of a checkerboard structure with resistivities of 10 and 100 Ω m and a size of 80 km × 80 km embedded in the lower crust layer (from the depth of 14.8 to 33.3 km of the layered-earth model shown in Fig. 2a). An array of 25 irregularly distributed MT stations (*crosses*) covers the area of interest, which is 160 km × 160 km (*dashed frame*). Here, one MT station represents an area of 32 × 32 km (*dash-dotted frames*)

was confirmed by another calculation with a smaller mesh. The diagonal elements of synthetic undistorted impedances are smaller in magnitude than that of the off-diagonal elements by a few orders of magnitude (Figure S9 in Section 3 of the Additional file 1). The det and ssq impedances from this array are shown in Fig. 9a, b, respectively. The frequency-dependent variation due to the embedded anomalies can be recognized both for the det and ssq impedances.

To obtain distorted 3D synthetic data, the randomly generated distortion tensors used in the 1D example were applied to the synthetic data from this array. When the MT impedance is distorted, the diagonal elements become significant and can be comparable to the off-diagonal elements (Figure S10 in Section 3 of the Additional file 1). In the 3D situation, the effect of the distortion parameters on the rotational invariants is different from that in the 1D case because the near-surface distorter causes a static shift and phase mixing, i.e., mixing among the different elements of the MT impedance tensor. An example of the rotational invariants from the distorted data is shown in Fig. 10a. The ssq impedance is shifted upward (because of the site gain at this station) and contains a frequency dependence, as demonstrated by differences in the magnitude and phase derived from the distorted and undistorted ssq impedances (Fig. 10b). Unlike the ssq impedance, only the magnitude of the det impedance is affected by the distortion. From Fig. 10b, the magnitude of the det impedance is biased downward because the impedance at this site is distorted by the shear and splitting parameters, whereas its phase remains unchanged.

All det and ssq impedances distorted by distortion parameters with an SD of 0.3 from this array are shown in Fig. 11. The difference between those using the distorted det impedances and those using the distorted ssq impedances is clear when they are averaged (Fig. 12). Here, the error bars indicate the SD. At the same distortion strengths (SD), the average ssq impedances have smaller SDs than the det impedances, which is the same as in the 1D case. This also confirms that the ssq impedance is less sensitive to galvanic distortion. Consequently, the apparent ssq gain (Section 6) should be a good approximation of the site gain. In addition, the approximations that the effects of the dimensionality and geometric distortion would be minor after averaging over a number of MT stations, which is applied in Eq. (17) of Rung-Arunwan et al. (2016), have been verified with the calculation detailed in Section 2 of the Additional file 1.

Next, we inverted the average det and ssq impedances to obtain models of the regional mean 1D profiles for different cases with the same criteria used in the 1D examples. Because the average det and ssq impedances from the undistorted data are similar, the models derived from them

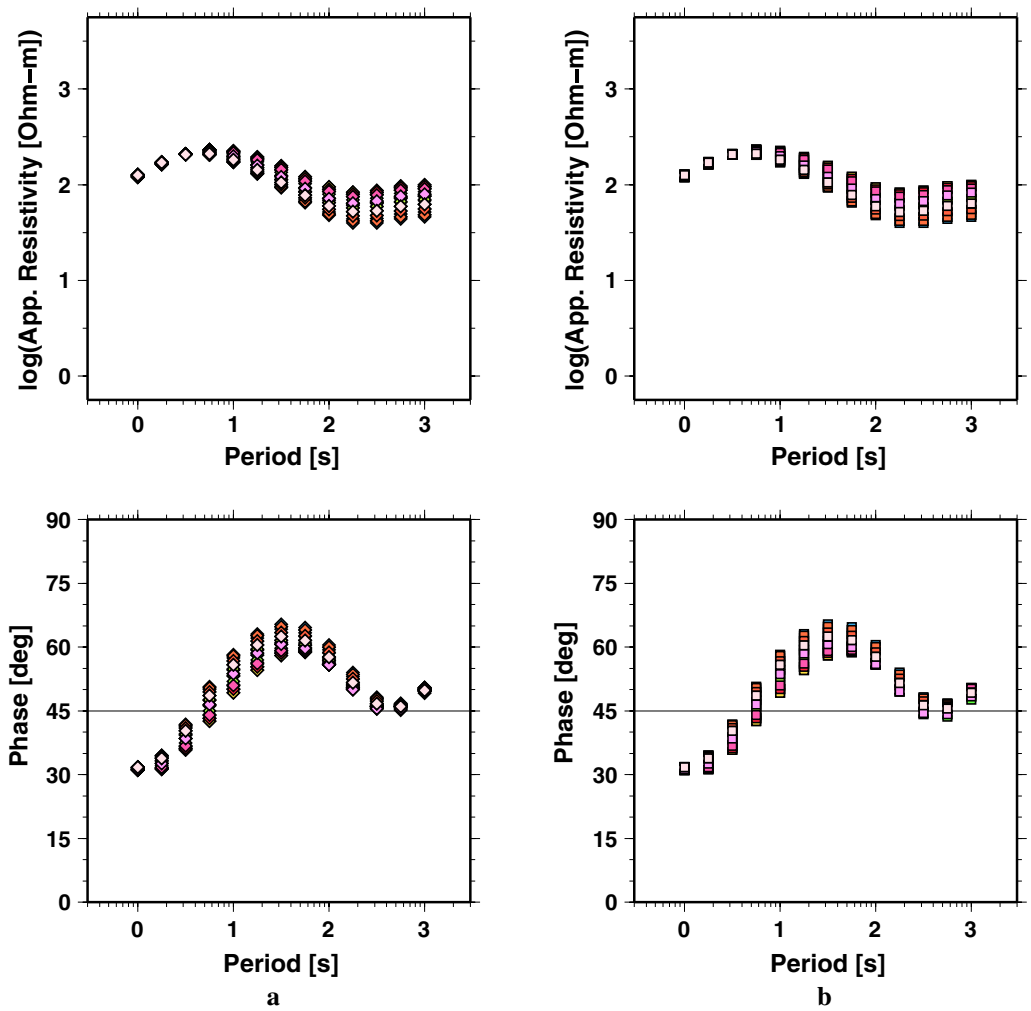

Fig. 9 **a** Det and **b** ssq impedances from the array of MT stations over the 3D anomalies (Fig. 8) without galvanic distortion. Each station is represented by a different *symbol color*

are approximately the same (Fig. 13). These models are also consistent with the theoretical models of the mean 1D profile, which were calculated by applying Eqs. (3) and (4) to the conductivity distribution within the area of interest in this setting (dashed frame in Fig. 8). However, with the presence of galvanic distortion, the models of the mean 1D profile derived from the average det impedances tend to be more conductive. Conversely, at any distortion strength, the average ssq impedances yield models of the regional mean 1D profile that are close to the undistorted one. Nonetheless, we should note that this result is obtained simply because the array size is sufficiently larger than the typical anomaly size. In the 3D situation, estimation of the regional mean 1D profile could be affected by the size of the observation array and its location relative to the location of the anomaly, even if the same number of observation sites is involved. We will examine these issues in the next section.

Examination of the consistency between the theoretical and estimated models of the regional mean 1D profile

According to the fact that the host layer earth or background is absolutely unknown in reality, the estimated models of the regional mean 1D conductivity profiles from 3D models should not be compared with the synthetic layered-earth model (the model in Fig. 2a, for example). Instead, it should be compared with the theoretical regional mean 1D conductivity profiles, the linear and logarithmic averages of the lateral conductivity distribution (Eqs. 3 and 4). Obviously, the regional mean 1D profiles, either theoretical or estimated, depend on the array size and location when the subsurface structure is laterally heterogeneous. This section aims to examine the consistency between the defined and estimated models of the regional mean 1D profile and the effect of the

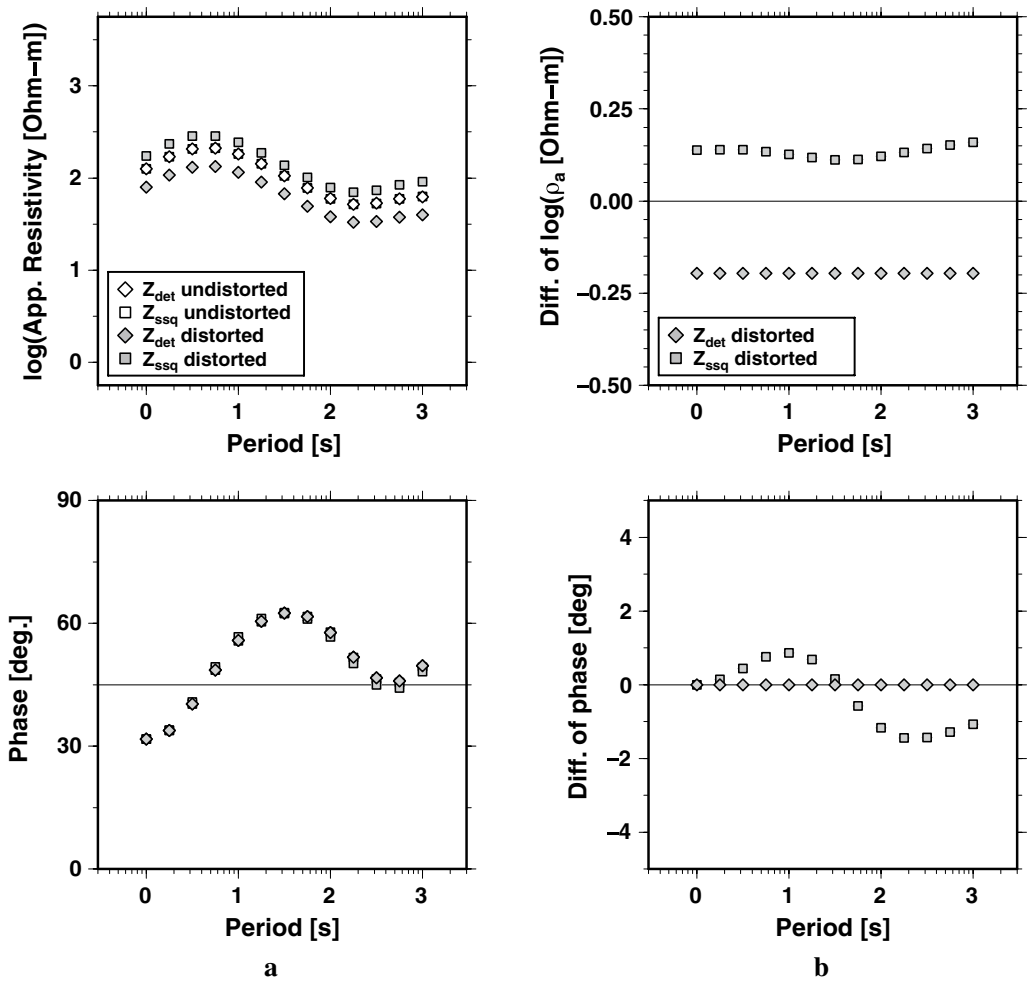

Fig. 10 **a** Example of det and ssq impedances from station `syn08` distorted with $(g, t, e, s) = (1.20, 0.11, -0.37, 0.49)$. **b** Difference between the distorted and undistorted rotationally invariant impedances

consistency on the location of the array and its size relative to the anomaly size through synthetic modeling.

We again use the model of the checkerboard structure, as described in Section 3.2. In the first example, the observation array is also the same, i.e., 25 MT stations within an area of 160 km × 160 km, but the arrays are set in three different locations at central, northwest, and northeast locations (Fig. 14). At the central location, the array is concentric with the anomaly intersection, whereas at the northwest and northeast locations, the arrays are centered over the 10 and 100 Ω m anomalies, respectively.

As shown in the previous sections, the det impedance is biased by the geometric distortion (shear and splitting) so that the ssq impedance is only considered in the following. The average ssq impedances from these arrays were calculated and inverted in the same manner as described in Section 3.2. The theoretical models of the mean 1D profile (Fig. 15a) were calculated using Eq. (3) or (4) from the conductivity distribution within the area of the observation array (e.g., the dashed frames in Fig. 14). The MT responses from the theoretical models (Fig. 15b) were then calculated using the analytical solution (see Chave and Jones 2012).

In this situation, where the array is much larger than the typical anomaly, the regional mean 1D conductivity profiles from different array locations, both theoretical and estimated, are shown to be almost identical to the theoretical model. This is also a consequence of the application of the averaging approach, in which the effects of the positive and negative anomalous conductivities are averaged out. In other words, the theoretical and estimated models of the regional mean 1D profile are nearly independent of the array location when the array size is much larger than the typical anomaly size.

Next, to demonstrate the effect of the array size, we decrease the size of each array to 80 km × 80 km (Fig. 16),

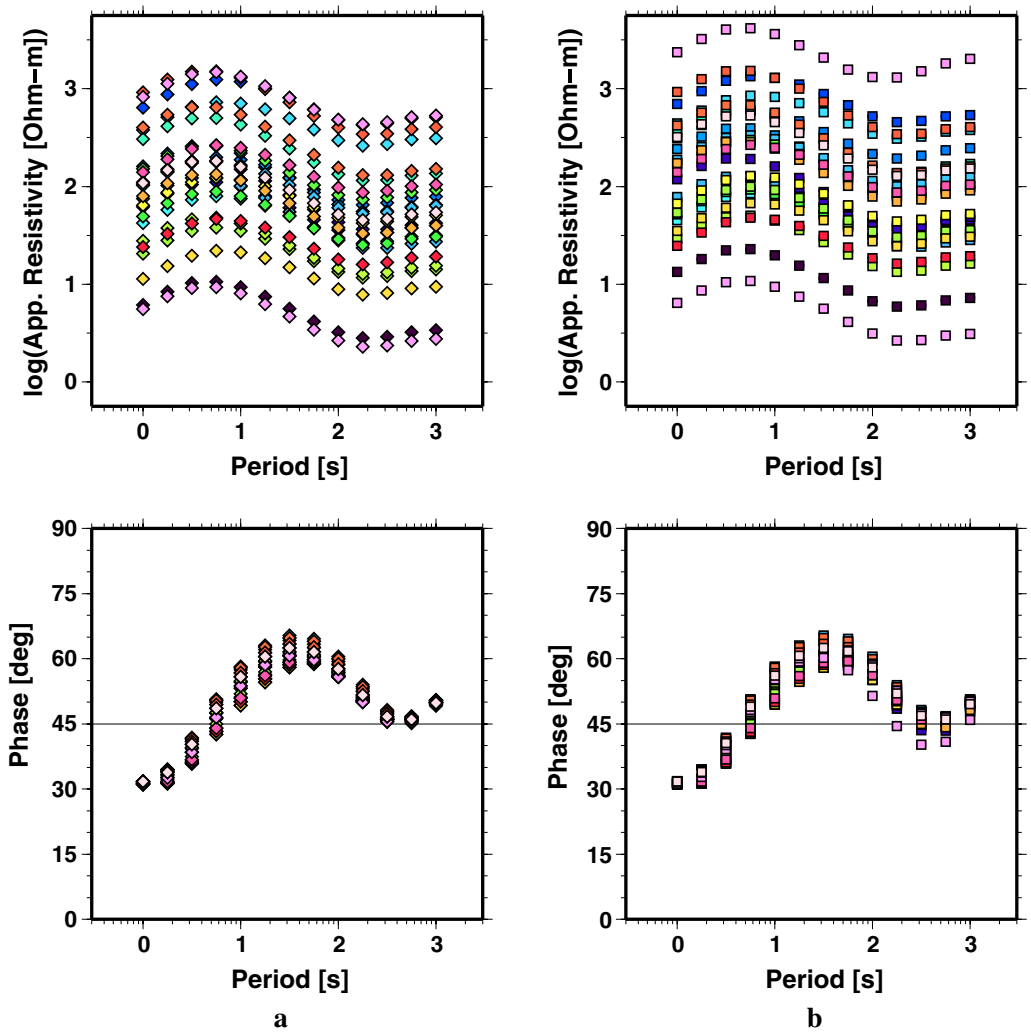

Fig. 11 **a** Det and **b** ssq impedances from the 3D example (as shown in Fig. 9a, b, respectively) distorted with a set of distortion parameters with an SD of 0.3

which is equal to the anomaly size. From this setting, the estimated results are shown to be spatially dependent (Fig. 17). Moreover, the inconsistency between the theoretical and estimated models of the regional mean 1D profiles is evident, particularly in the layer where the anomaly is embedded (Fig. 17). The inconsistency becomes more obvious if the array size is further reduced. This is a consequence of the inappropriate design of the observation array, i.e., it is not large enough to cover the structure of interest. However, having an array with an appropriate size and site spacing may be difficult in reality without any a priori knowledge because the size of structure is usually unknown beforehand. Thus, the estimation of the mean 1D profile with a larger array would be more reliable.

In general, the observation array should be designed to cover the structure of interest if its size is known a priori. However, if the anomaly size is found *a posteriori* to be comparable to or even larger than the size of observation array, 3D inversion of any approach will fail to accurately image the heterogeneity. To obtain more reliable results, one suggestion in such a case is to add more MT observations to make the array size sufficiently greater than the anomaly size.

Local and regional distortion indicators

On the basis of the fact that the galvanic distortion has different effects on the det and ssq impedances, the LDI and RDI given by Eqs. (8) and (9), respectively, were constructed to quantify the strength of the geometric

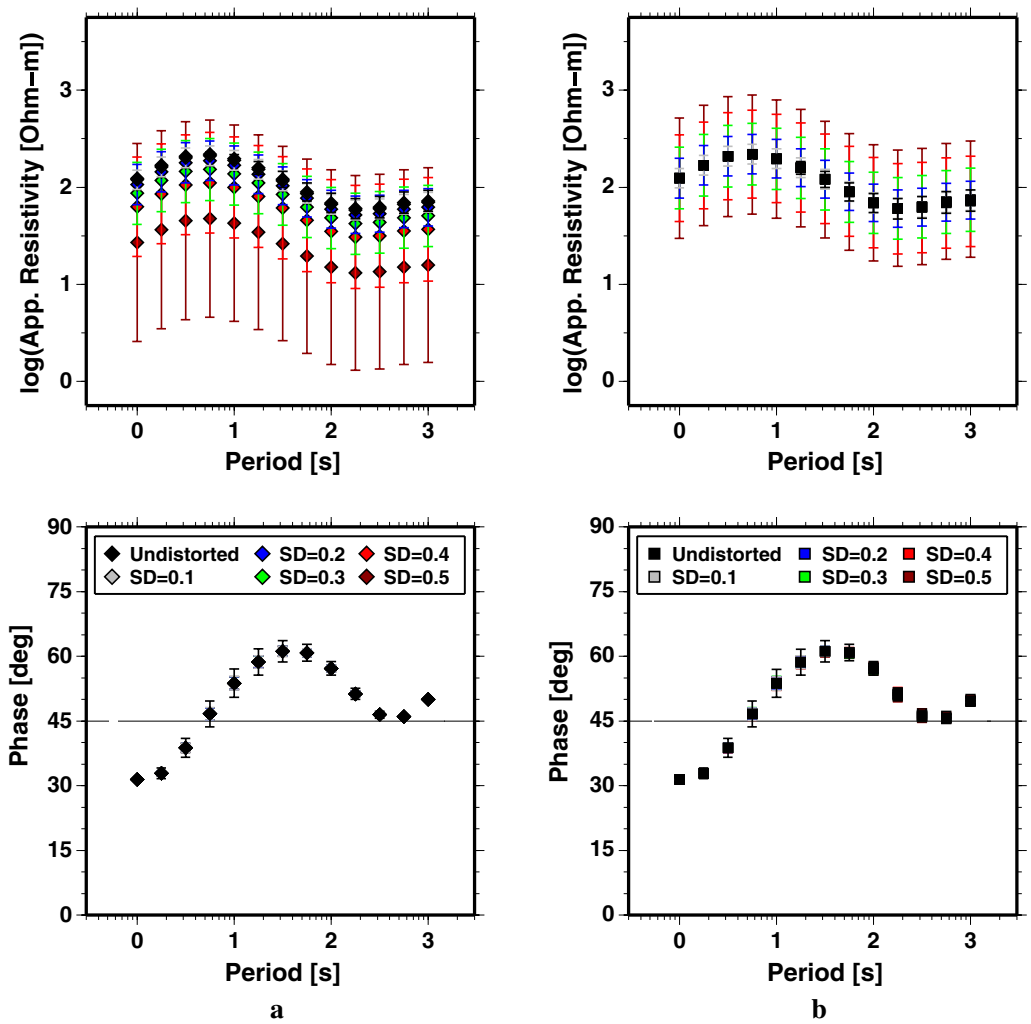

Fig. 12 Average **a** det and **b** ssq impedances from the 3D datasets distorted with different galvanic distortion strengths

distortion that can be described by the shear and splitting parameters. This section examines the numerical results of LDIs and RDIs derived from the synthetic 1D and 3D examples presented in Sections 3.1 and 3.2, respectively.

For the 1D case without distortion, where the det and ssq impedances are identical, the LDI is unity. However, when the impedances are distorted, the LDIs from the 1D example are shifted upward (larger than unity) but remain real-valued (Fig. 18a). Larger LDIs correspond to stronger geometric distortions at the MT sites. The 3D anomalies at the depth of interest cause a frequency-dependent difference between the det and ssq impedances because of the inductive effect. The LDIs then become frequency-dependent and complex-valued (Fig. 18b), but the effect of the geometric distortion dominates.

The RDIs also show features similar to the local ones. In the 1D case, the RDIs are shifted upward depending on the distortion strength throughout the dataset (Fig. 19a). Thus, the RDI will be able to tell whether or not a simple galvanic distortion model is applicable to the given dataset. In contrast to the LDI, the frequency-dependent features from the 3D effect are smoothed, as shown in Fig. 19b, such that the RDIs are almost real-valued and weakly frequency-dependent if the distortion is purely galvanic.

For practical usage of the LDI, we calculate the mean LDI $\bar{\gamma}_i$ as the geometric average of the real part of the LDIs over a given period range. The real part chosen as the LDI is a real-valued number in cases of 1D earth. At the ith station,

$$\bar{\gamma}_i = \left[\prod_{j=1}^{M} \Re\, \gamma_i(\omega_j) \right]^{\frac{1}{M}}, \tag{13}$$

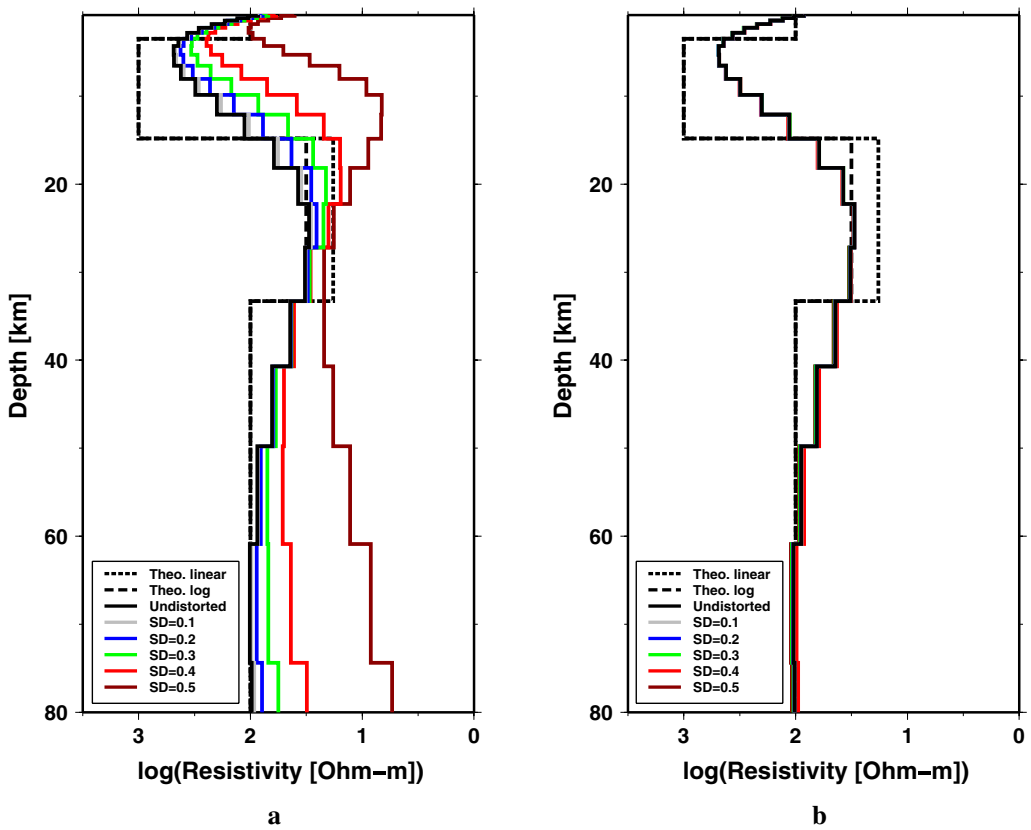

Fig. 13 1D models inverted from the average **a** det and **b** ssq impedances from the distorted 3D datasets (Fig. 12). The theoretical models of the mean 1D profiles, $\sigma_R(z)$, from this setting with both linear (Eq. 3) and logarithmic (Eq. 4) scaling (*black dashed lines*) and the 1D model from the undistorted data (*black solid line*) are shown for comparison

where M is the number of periods. The percentage error in the mean LDI is calculated with

$$\mathcal{P}(\bar{\gamma}_i) = \frac{\bar{\gamma}_i - \gamma_i}{\gamma_i} \times 100\%, \tag{14}$$

where the synthetic LDI is calculated using

$$\gamma_i = \frac{(1+e_i^2)(1+s_i^2)}{(1-e_i^2)(1-s_i^2)}.$$

As the LDI correctly estimated the integrated effect of shear and splitting in 1D cases, their means (Eq. 14) are not shown here. However, as shown earlier, the underlying structures affect the LDIs (Fig. 18b) if they are not 1D. The mean LDIs from the 3D example may include some error in the estimate of the effect of the geometric distortion at each station (Fig. 20). The error bars of the mean LDIs (Fig. 20b) here are set to the SD of the real part of the mean LDI in order to represent the dispersion in the frequency-dependent part contributed by the underlying structure.

One possible practical usage of the LDI is the omission of some stations with heavily distorted impedances from the interpretation or inversion if the number of such sites is small. If a limited number of sites showing heavy distortion are removed, the RDI after removal is supposed to be small. Conversely, if the RDI still exhibits a high value, a proper treatment for the galvanic distortion, such as inversion including the galvanic distortion (e.g., DeGroot-Hedlin 1995; Ogawa and Uchida 1996; Sasaki and Meju 2006; Avdeeva et al. 2015) or an MT data analysis (e.g., Weaver et al. 2000; Caldwell et al. 2004), will be essential. The combination of LDIs and RDI helps to provide insight, at least to some extent, as to which approach should be applied to a set of MT impedances obtained from observation.

Apparent gains

From the theoretical derivation, the apparent ssq gain is expected to correctly estimate the site gain in 1D cases and to yield a good approximation of it in 3D cases, whereas the apparent det gain underestimates the

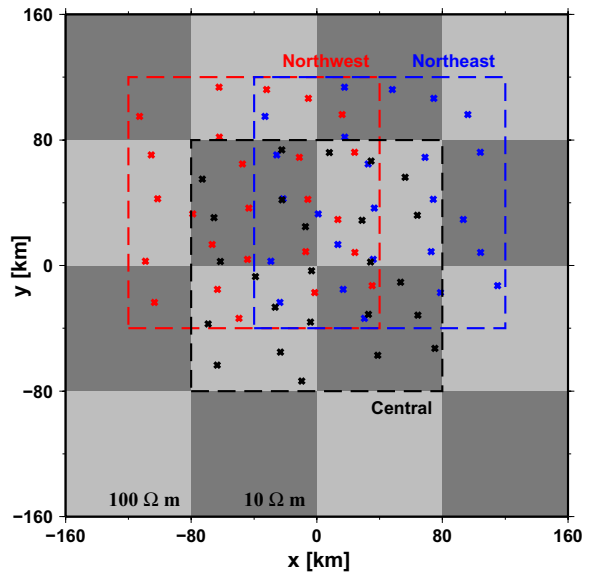

Fig. 14 Checkerboard structure with an anomaly size of 80 km × 80 km and resistivities of 10 (*dark gray*) and 100 (*light gray*) Ω m. The checkerboard structure was embedded in the lower crust layer (from a depth of 14.8 to 33.3 km in the layered-earth model shown in Fig. 2a). *Three arrays* of 25 MT stations (*crosses*), each with a size of 160 km × 160 km (*dashed frames*), were placed at central (*black*), northeast (*blue*), and northwest (*red*) positions

synthetic site gain if the data are strongly affected by geometric distortion. In this section, we demonstrate the use of the apparent gains obtained from the synthetic 1D and 3D examples described in Sections 3.1 and 3.2, respectively.

From our 1D example, the apparent ssq gain (Eq. 11) perfectly agrees with the synthetic site gain, but the apparent det gain (Eq. 10) is biased downward, as expected (Fig. 21a). Here, the error bars of the apparent det and ssq gains are derived from the SD when estimating the regional averages of the det and ssq impedances, $\bar{Z}'_{\mathrm{det}}$ and $\bar{Z}'_{\mathrm{ssq}}$ in Eqs. (6) and (7), respectively. However, in the 3D case, the induction effect of the 3D heterogeneity, which can be observed in the frequency-dependent features of both the magnitude and phase (Fig. 21b), is included. For example, the apparent ssq gain from the station `syn08` (Fig. 21b) is biased downward and then underestimates the synthetic site gain in the period range where the induction from the underlying regional conductive anomaly is effective. Moreover, a variation in the apparent gains among different sites due to the underlying 3D structure is observed (Fig. 23). However, the apparent ssq gain still agrees with the synthetic site gain within the standard error.

To meaningfully interpret these results, we calculated the mean apparent det and ssq gains, $\bar{g}_i^{\mathrm{det}}$ and $\bar{g}_i^{\mathrm{ssq}}$, using the geometric mean of the real part of the apparent gains over a given period range (as with Eq. 13). Only the real part was used to ensure consistency with the mathematical assumption that the distortion operator is a 2×2 tensor of real-valued numbers. Given that the number of periods where the impedances were obtained at each station is M, the mean apparent gains can be written as

$$\bar{g}_i^{\mathrm{det}} = \left[\prod_{j=1}^{M} \Re g_i^{\mathrm{det}}(\omega_j) \right]^{\frac{1}{M}} \tag{15}$$

and

$$\bar{g}_i^{\mathrm{ssq}} = \left[\prod_{j=1}^{M} \Re g_i^{\mathrm{ssq}}(\omega_j) \right]^{\frac{1}{M}}. \tag{16}$$

The mean apparent gains estimated at synthetic MT sites from 1D and 3D examples are all presented in Figs. 22a and 23a, respectively. The percentage differences between the mean apparent gains and the synthetic site gains are shown in Figs. 22b and 23b, respectively. They are given by

$$\mathcal{P}(\bar{g}_i^{\mathrm{det}}) = \frac{\bar{g}_i^{\mathrm{det}} - g_i}{g_i} \times 100 \tag{17}$$

and

$$\mathcal{P}(\bar{g}_i^{\mathrm{ssq}}) = \frac{\bar{g}_i^{\mathrm{ssq}} - g_i}{g_i} \times 100, \tag{18}$$

where g_i is the synthetic site gain at the ith station. In spite of the large site-to-site variation in the synthetic site gain of nearly one order of magnitude (two orders of magnitude in terms of the static shift in the apparent resistivity), its estimation error by the mean apparent ssq site gains is as small as only a few percent.

The mean apparent gains from the 1D example are shown in Fig. 22a. The error bars in this figure are derived from the error propagation in calculating the mean of the apparent gain at each station. In this case, the mean apparent ssq gains and synthetic site gains are the same for every MT observation (Fig. 22b). Conversely, the apparent det gain may either underestimate or overestimate the synthetic site gain depending on the strength of the local galvanic distortion.

Unlike the 1D case, the existing 3D anomalies may cause further uncertainty, as the apparent ssq gain has been demonstrated to be affected by the induction effect from the underlying 3D structure. For example, the mean apparent ssq gains from stations over the conductive structure (e.g., stations `syn07` and `syn19`) tend to be

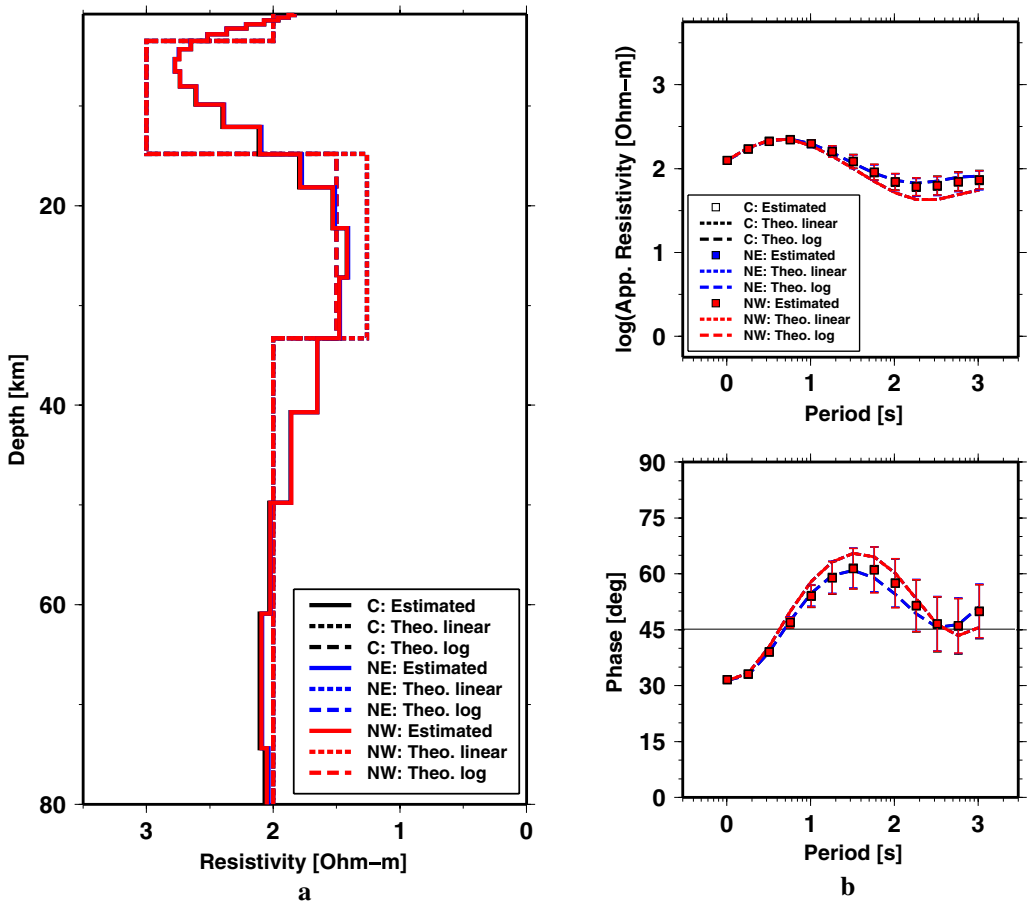

Fig. 15 **a** Theoretical (*dashed lines*) and estimated (*solid lines*) models of the mean 1D profiles obtained using the settings shown in Fig. 14. **b** Corresponding MT responses from the theoretical (*dashed line*) and estimated (*squares*) models of the mean 1D profiles. The results obtained from different array locations—Central (C), Northwest (NW), and Northeast (NE)—are represented by *lines* and *symbols* of different *colors*

slightly smaller than the synthetic site gains (Fig. 23b). In spite of this, the percentage differences (Eq. 18) still remain about 10% which is within the statistical uncertainty (Fig. 23a). The regional distortion indicator in this case (Fig. 19b) shows a feature consistent with the distorted 1D case (Fig. 19a) at periods shorter than 15 s. If we estimate the mean ssq gain from this period band instead of Eq. (16), the percentage gain difference becomes as small as 5%.

In previous works, the site gain is considered or regarded to be an indeterminable distortion parameter if other independent geophysical data, e.g., transient electromagnetic (TEM) data (Beamish and Travassos 1992; Groom et al. 1993; Bibby et al. 2005; Árnason 2015), are not available. However, the TEM data may not be available at all MT stations. In addition, the static shift could be corrected with the TEM data with some limitations (see Watts et al. 2013; Tournerie et al. 2007; Wilt and Williams 1989), e.g., when the heterogeneity is smaller than the transmitter loop. Utada and Munekane (2000) attempted to solve this problem by introducing Faraday's law as a constraint, but the solution was not practical. The numerical examples presented here show that the concept of the apparent gain can be used to approximate the site gain in the assumed situation.

This paper considers the galvanic distortion caused only by small-scale heterogeneities (smaller than the typical site spacing and confined within a near-surface layer shallower than the inductive scale length of interest). Thus, the effect of galvanic distortion is considered as spatial aliasing in the MT data. The apparent gain can then be regarded as a shift in the magnitude of the impedance relative to the average value. For the case where the data are systematically shifted by some near-surface structure larger than or comparable to the array size (see Section 4), e.g., a valley environment such as of the Rhine Graben model (see Chp. 6 in Chave and Jones 2012), the apparent ssq gain may be distributed around

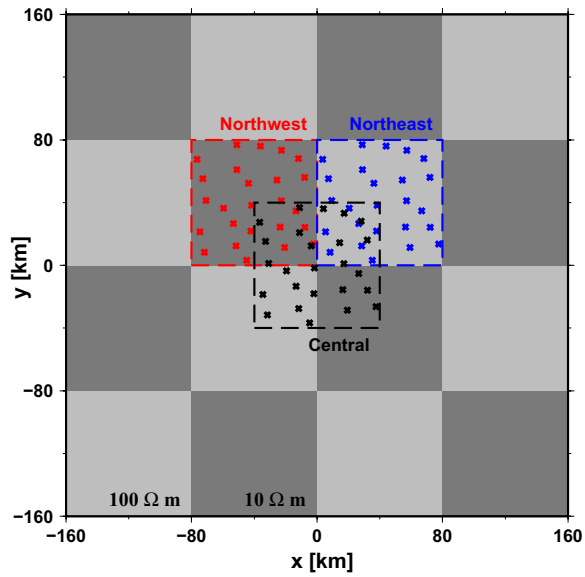

Fig. 16 Same as Fig. 14 for an array size of 80 km × 80 km

some biased central values or may not be normally distributed on a logarithmic scale. In such cases, the concept of the apparent gain should be used with caution.

Dependence on the distortion model

The proposed method (Rung-Arunwan et al. 2016) is theoretically formulated on the basis of the Groom–Bailey model of galvanic distortion. In this paper, it is shown numerically that the use of the average ssq impedance is a reliable method for estimating the regional mean 1D conductivity profile, and the combination of the two rotational invariant impedances helps to detect the geometric distortion and to approximate the site gain. Although the Groom–Bailey model is well known and adopted by a number of studies, it is not the only model. The distortion operator $\mathbf{C}$ can be parameterized using other models (e.g., Bahr 1988; Chave and Smith 1994; Smith 1995; Tietze et al. 2015). Therefore, the galvanic distortion model dependence of the proposed methods may be questionable.

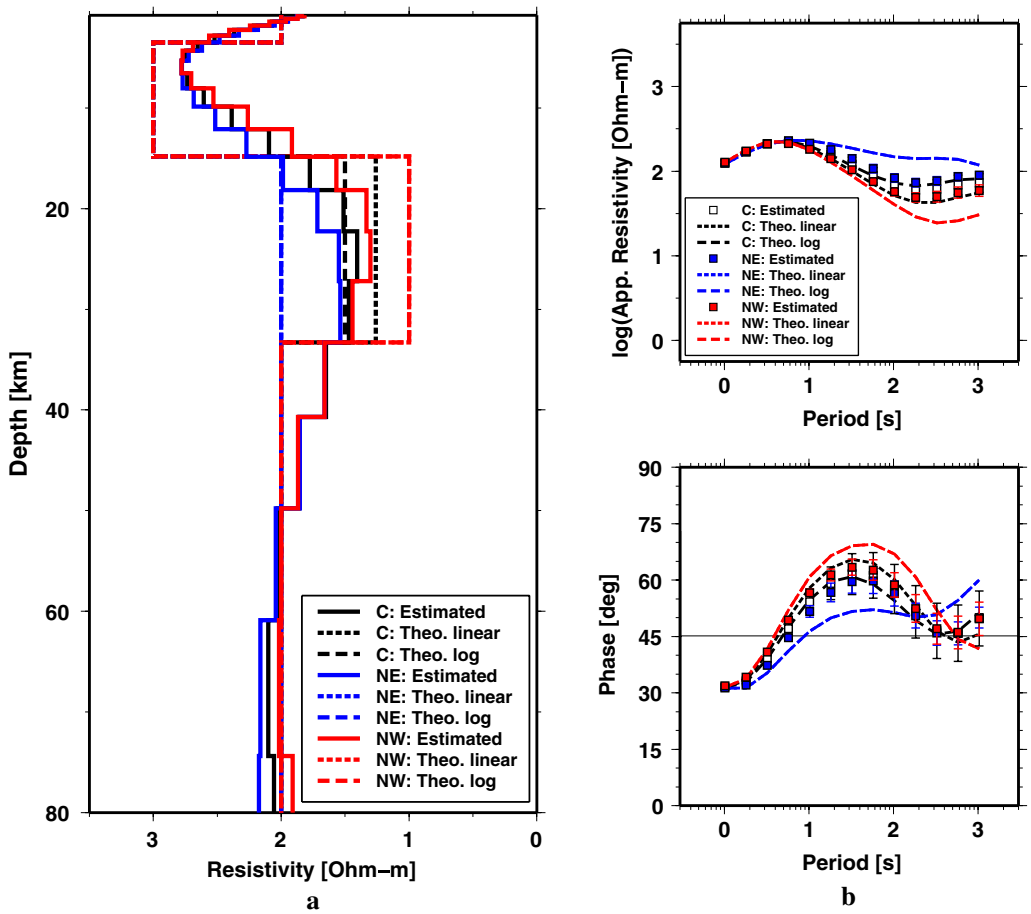

Fig. 17 **a** and **b** Same as Fig. 15 for the settings shown in Fig. 16

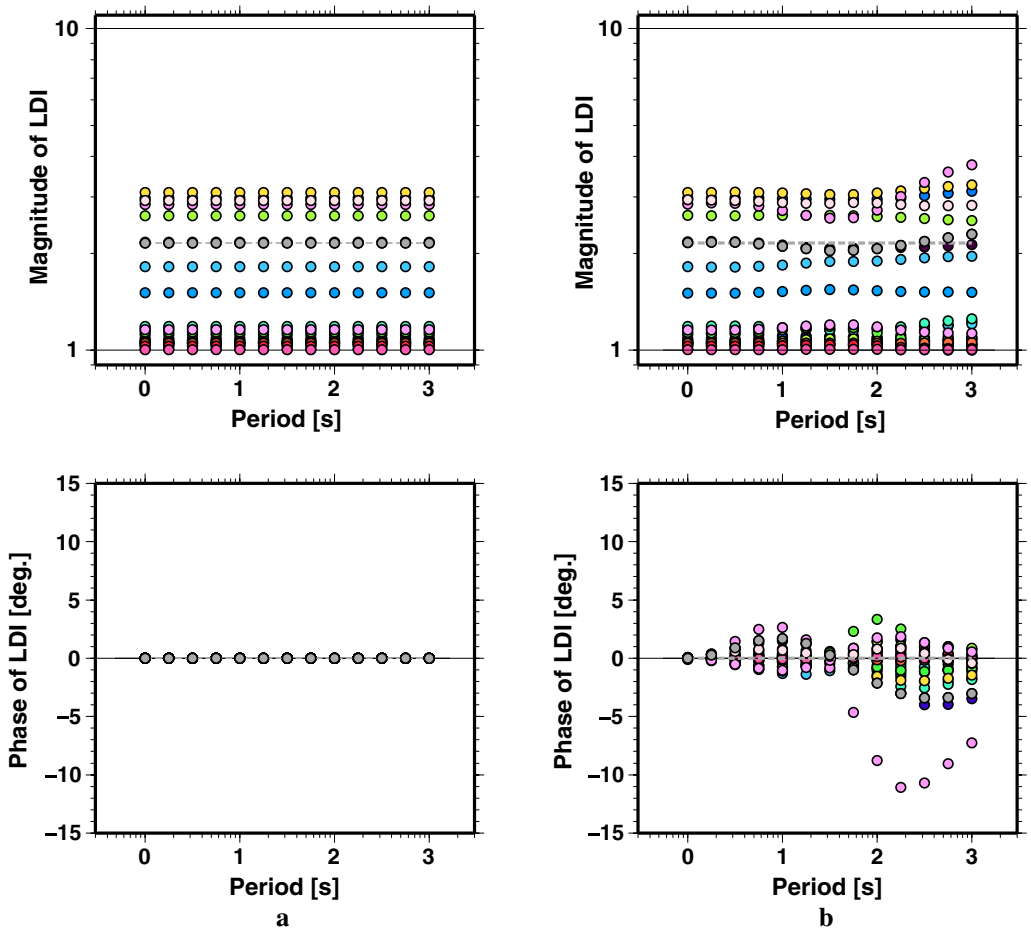

Fig. 18 LDIs from the distorted **a** 1D and **b** 3D data (in '1D example', '3D example' sections, respectively), where a set of distortion parameters with an SD of 0.3 was applied. Examples of 1D and 3D data at station `syn08` distorted with $(g, t, e, s) = (1.20, 0.11, -0.37, 0.49)$ (*gray circles*) are compared with the synthetic values of the LDI at this station (*dashed lines*)

In this section, we examine the galvanic distortion model dependence of the proposed methods by using the perturbed identity matrix (PIM) model for the distortion operator, which has been recently introduced to model the galvanic distortion (e.g., Tietze et al. 2015). Like the Groom–Bailey model, the PIM model has four degrees of freedom. In the PIM model, the distortion operator $\mathbf{C}$ is expressed as the perturbation of the identity matrix, i.e., $\mathbf{C} = \mathbf{I} + \mathbf{D}$, where $\mathbf{I}$ is a 2×2 identity matrix, and $\mathbf{D}$ is a 2×2 perturbation matrix describing the distortion. In the test, we simulate an array of 25 MT stations over 1D earth, as in Section 3.1. The 25 cohorts of $\mathbf{D}$ elements are to be normally distributed random numbers with various SD levels, and the distortion operators are then formed and applied to the 1D impedance tensors (Section 3.1). The average det and ssq impedances from the distorted data are calculated. Figure 24a shows the average impedances for the case with an SD of 0.5. The average det and ssq impedances are then inverted in the same manner as in Section 3.1, and the resulting 1D models are shown in Fig. 25. As expected by our theory, the average det impedance gives an underestimate of the regional mean 1D conductivity profile, while the average ssq impedance depends less on the distortion.

Approaches for detecting the galvanic distortion are also effective for the PIM model. The LDIs from the dataset distorted using $\mathbf{D}$ are shown in Fig. 24b. The LDIs in the PIM model are consistent with the theoretical expectation that they are greater than unity if geometric distortion exists, and their magnitudes represent the distortion strength. The concept of the apparent gain is also applicable under the PIM model. The apparent ssq gains from different stations and their mean values (Fig. 26) are calculated using Eqs. (11) and (16), respectively. They seem consistent with the Frobenius gain, the gain derived from the Frobenius norm of the distortion tensor $\mathbf{C}$ (see Bibby et al. 2005), although the Frobenius gains are neither normally distributed nor have zero mean (Additional file 1:

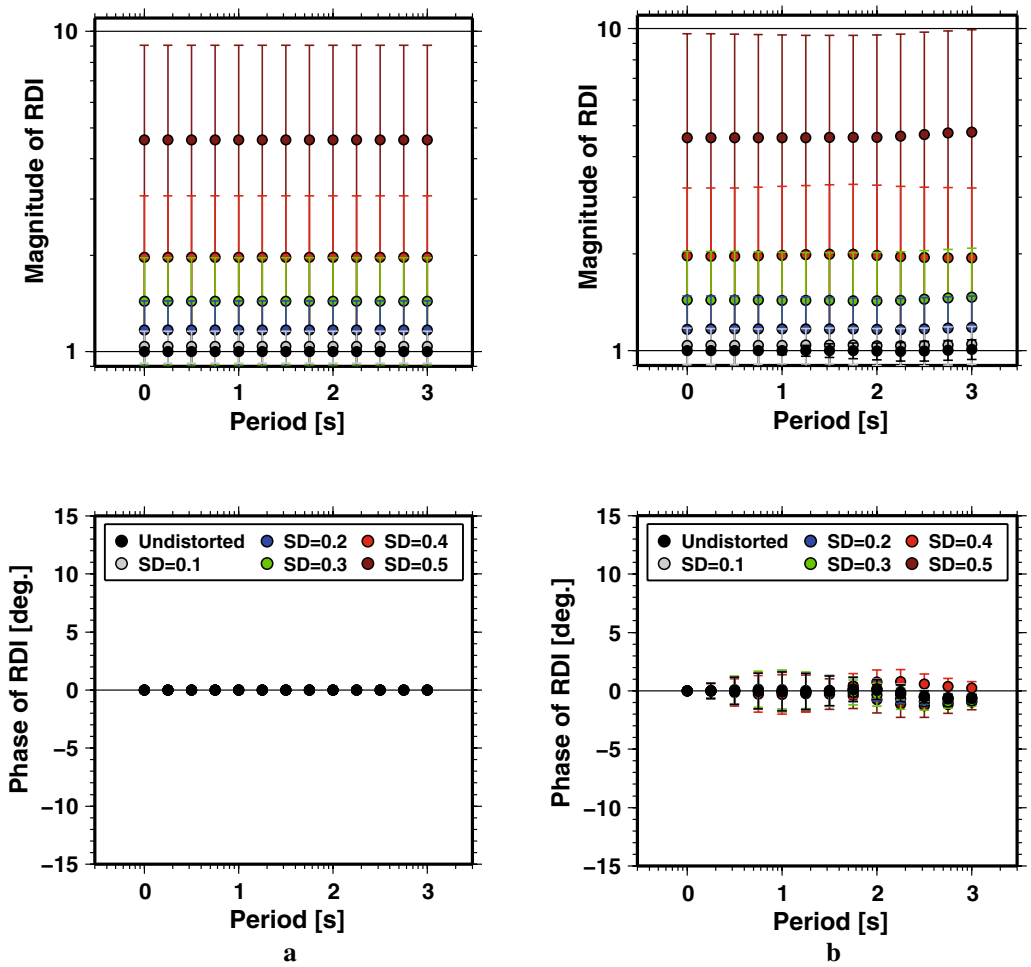

Fig. 19 RDIs from **a** 1D and **b** 3D examples with different galvanic distortion strengths

Figure S16). It is shown that the apparent ssq gain still gives a good approximation of the site gain under the PIM model.

Under the PIM model, the site gain is likely to have a skewed distribution, which can compensate for the downward bias of det impedances caused by geometric distortion (shear and splitting), e.g., the case of weak distortion in the PIM model. Therefore, it is possible that there may be a case where the average det impedance is more appropriate than the average ssq impedance for a particular condition. However, searching for a special case where the skewed site gain and the bias due to the geometric distortion are balanced is out of the scope of this paper.

From results shown above, it is clear that the proposed method does not strongly depend on the choice of galvanic distortion model. The use of the average ssq impedance is a promising method for estimating the regional mean 1D conductivity profile and a good approximation for the site gain. The results confirmed that a combination of the rotational invariants (det and ssq) is useful for detecting the galvanic distortion. More details of the PIM model test can be found in Section 4 of the Additional file 1.

Conclusions

This paper presents numerical examples of the properties and galvanic-distortion-related parameters (a model of the regional mean 1D conductivity profile, the local and regional distortion indicators, and the apparent gains) that can be obtained from a set of distorted MT impedances. By correcting the traditional Berdichevsky average, this study has shown that a model of the regional mean 1D profile can be correctly estimated by using the average ssq impedance. Regardless of the galvanic distortion strength, the average ssq impedance

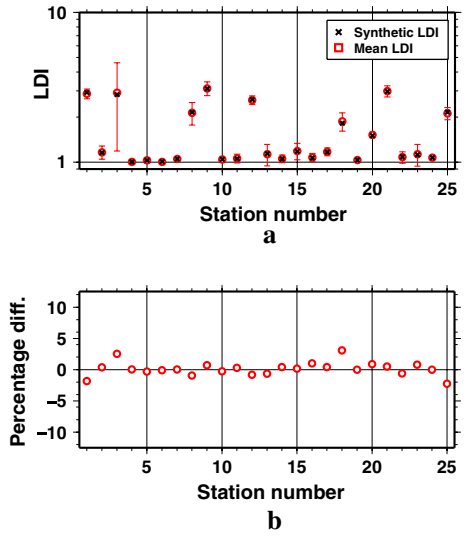

Fig. 20 **a** Comparison of synthetic LDIs (*black crosses*) with the mean LDIs (*red circles*) from the 3D example, where a set of distortion parameters with an SD of 0.3 was applied. **b** Percentage difference between the mean LDIs and the synthetic values

gives a reliable model of the regional mean 1D conductivity profile. The local and regional distortion indicators were defined to detect the effects of the shear and splitting parameters in the Groom–Bailey model of galvanic distortion, and the apparent gains were used to approximate the magnitude of the site gain in some cases presented in this paper. The use of these parameters may help to quantify the intensity of the galvanic distortion contained in MT data and determine the need for the proper treatment of the galvanic distortion. For example, if the distortion in a given dataset is proven to be solely caused by the site gain, only gain correction is required. In addition to gain correction, if the data at only a few stations include strong geometric distortion, as revealed by the local and regional distortion indicators, the data could be omitted or weighted less during 3D inversion. Note that a model of galvanic distortion is applicable for a particular frequency band where the distortion is expressed by a real-valued 2×2 tensor. This can be tested by checking whether the apparent ssq gain and LDI are real-valued and almost

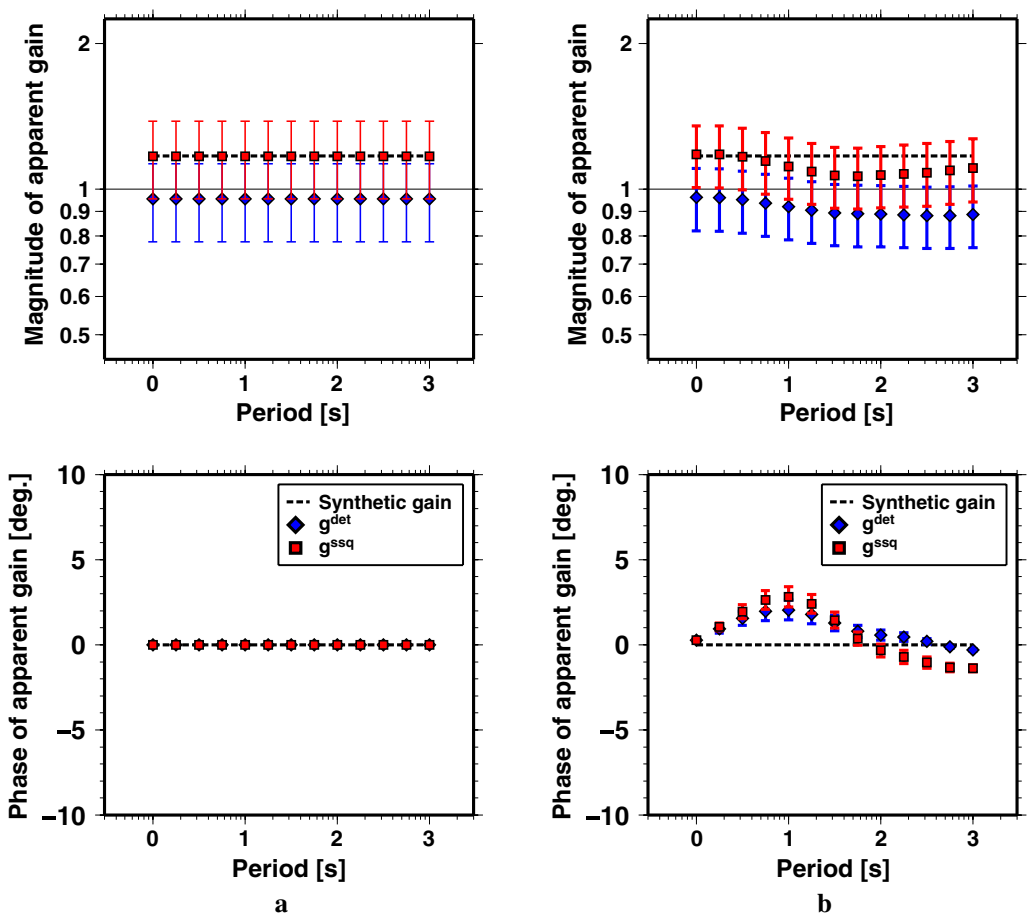

Fig. 21 Det (*diamonds*) and ssq (*squares*) apparent gains from **a** the 1D example and **b** station `syn08` in the 3D example. A synthetic site gain (*dashed line*) of 1.20 was applied at this station

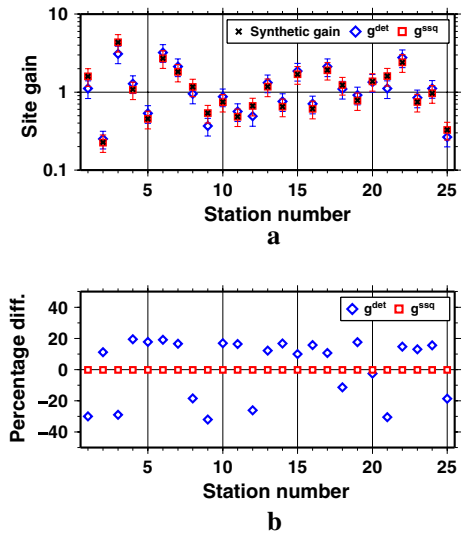

Fig. 22 **a** Comparison of synthetic site gains (*crosses*) with the mean apparent det (*diamonds*) and ssq (*squares*) gains from the 1D example, where a set of distortion parameters with an SD of 0.3 was applied. **b** Percentage difference between the mean apparent gains and the synthetic site gains

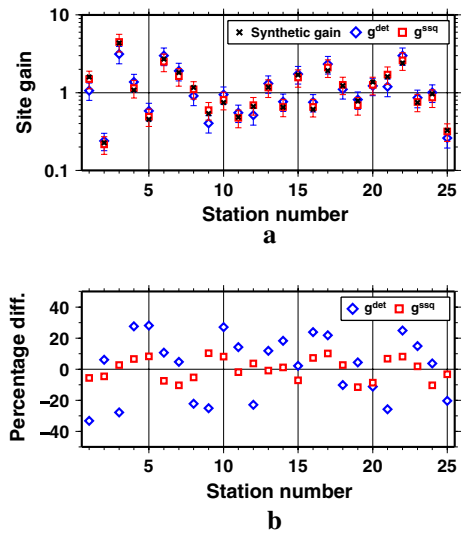

Fig. 23 **a** and **b** Same as Fig. 22 for the 3D example

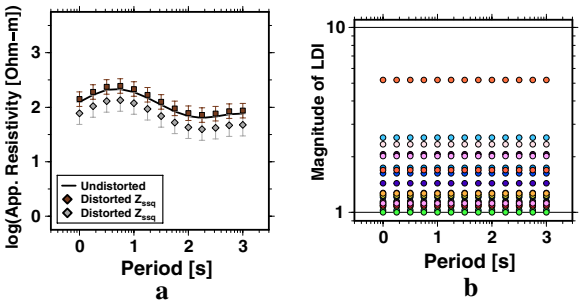

Fig. 24 **a** Average det (*diamonds*) and ssq (*squares*) impedances from the dataset distorted under the PIM model, where the elements of the perturbation matrix **D** are normally distributed random numbers with an SD of 0.5. They are shown in comparison with the undistorted 1D response (*black solid line*), which is as shown in Fig. 2b. **b** Local distortion indicators from this dataset

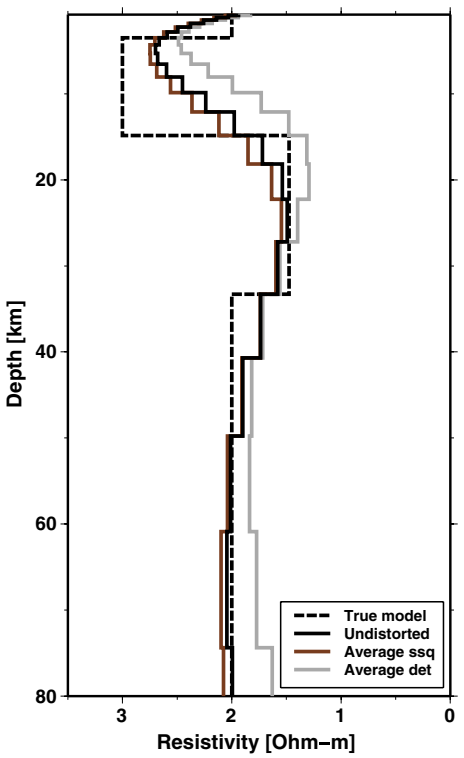

Fig. 25 1D models inverted from the average det and ssq impedances shown in Fig. 24a in comparison with the model inverted from the undistorted data

frequency independent at each site. This test also shows that the LDI can be used to justify the use of the impedance phase tensor as well. Because the apparent gain is a good approximation of the site gain, it can be used as an initial guess for the static shift in a 3D inversion. All of the results of the present study would resolve several

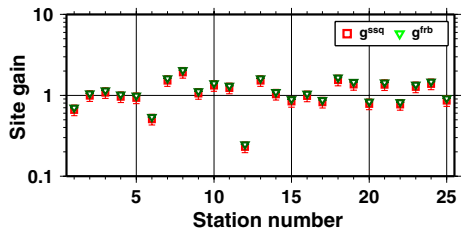

Fig. 26 Comparison of the gains derived from the Frobenius norm (*triangles*) with the mean apparent ssq gains (*squares*) from the 1D example, where the elements of the perturbation matrix **D** are normally distributed random numbers with an SD of 0.5

difficulties encountered during the inversion of a set of MT impedances that are contaminated by galvanic distortion.

Additional file

Additional file 1. Provides the synthetic experiments which (1) compare the arithmetic and geometric average, (2) support the approximation applied in the paper, (3) show the examples of all four elements of impedance tensors, and (4) examine the galvanic distortion model dependence of the proposed approaches.

Authors' contributions

TR conducted the numerical experiments and wrote this manuscript. WS critically revised this manuscript. HU provided basic ideas and critically revised this manuscript. All authors read and approved the final manuscript.

Author details

[1] Department of Physics, Faculty of Science, Mahidol University, 272 Rama 6 Road, Rachatawee, Bangkok 10400, Thailand. [2] Thailand Center of Excellence in Physics, Commission on Higher Education, 328 Si Ayutthaya Road, Bangkok 10400, Thailand. [3] Earthquake Research Institute, University of Tokyo, Yayoi 1-1-1, Bunkyo-ku, Tokyo 113-0032, Japan. [4] Present Address: Curl-E Geophysics Co., Ltd., 85/87 Nantawan Village, Uttayan-Aksa Road, Salaya, Phutthamonthon, Nakornpathom 73170, Thailand.

Acknowledgements

We wish to thank Yasuo Ogawa (the Editor), Ian Ferguson, one anonymous reviewer for constructive comments, and Alexey Kuvshinov for discussion. This work was partially supported by the Thailand Center of Excellence in Physics (ThEP) for WS and TR and was carried out as a part of an internship program for TR partially supported by the Earthquake Research Institute, the University of Tokyo. Most of the figures were produced using the Generic Mapping Tools (GMT) software (Wessel and Smith 1998).

Competing interests

The authors declare that they have no competing interests.

Publisher's Note

Received: 17 November 2016 Accepted: 31 May 2017
Published online: 14 June 2017

References

Arango C, Marcuello A, Ledo J, Queralt P (2009) 3D magnetotelluric characterization of the geothermal anomaly in the Llucmajor aquifer system (Majorca, Spain). J Appl Geophys 68(4):479–488
Árnason K (2015) The static shift problem in MT soundings. In: Proceedings world geothermal congress
Avdeev D (2005) Three-dimensional electromagnetic modelling and inversion from theory to application. Surv Geophys 26(6):767–799
Avdeeva A, Moorkamp M, Avdeev D, Jegen M, Miensopust M (2015) Three-dimensional inversion of magnetotelluric impedance tensor data and full distortion matrix. Geophys J Int 202(1):464–481
Baba K, Utada H, Goto TN, Kasaya T, Shimizu H, Tada N (2010) Electrical conductivity imaging of the Philippine Sea upper mantle using seafloor magnetotelluric data. Phys Earth Planet Inter 183(1–2):44–62 (Special Issue on Deep Slab and Mantle Dynamics)
Bahr K (1988) Interpretation of the magnetotelluric impedance tensor: regional induction and local telluric distortion. J Geophys 62:119–127
Beamish D, Travassos J (1992) A study of static shift removal from magnetotelluric data. J Appl Geophys 29(2):157–178
Berdichevsky M, Vanyan L, Kuznetsov V, Levadny V, Mandelbaum M, Nechaeva G, Okulessky B, Shilovsky P, Shpak I (1980) Geoelectrical model of the Baikal region. Phys Earth Planet Inter 22(1):1–11
Berdichevsky MN, Vanyan LL, Dmitriev VI (1989) Methods used in the U.S.S.R. to reduce near-surface inhomogeneity effects on deep magnetotelluric sounding. Phys Earth Planet Inter 53:194–206
Bibby HM, Caldwell TG, Brown C (2005) Determinable and non-determinable parameters of galvanic distortion in magnetotellurics. Geophys J Int 163:915–930
Boonchaisuk S, Siripunvaraporn W, Ogawa Y (2013) Evidence for middle Triassic to Miocene dual subduction zones beneath the Shan-Thai terrane, western Thailand from magnetotelluric data. Gondwana Res 23(4):1607–1616
Caldwell TG, Bibby HM, Brown C (2004) The magnetotelluric phase tensor. Geophys J Int 158:457–469
Chave AD, Jones AG (2012) The magnetotelluric method theory and practice, 1st edn. Cambridge University Press, Cambridge
Chave AD, Smith JT (1994) On the electric and magnetic galvanic distortion tensor decompositions. J Geophys Res 99(B3):4669–4682
Constable SC, Parker RL, Constable CG (1987) Occam's inversion: a practical algorithm for generating smooth models from electromagnetic sounding data. Geophysics 52(3):289–300
DeGroot-Hedlin C (1995) Inversion for regional 2-D resistivity structure in the presence of galvanic scatterers. Geophys J Int 122(3):877–888
Department of Mineral Resources D (2006) Active fault map in Thailand 1:1,000,000. Tech. Rep, Department of Mineral Resources, Bangkok, Thailand
Falgàs E, Ledo J, Marcuello A, Queralt P (2009) Monitoring freshwater-seawater interface dynamics with audiomagnetotelluric data. Near Surf Geophys 7(5–6):391–399
Gómez-Treviño E, Hernández FJE, Jones JMR (2013) Effect of galvanic distortions on the series and parallel magnetotelluric impedances and comparison with other responses. Geofís Int 52(2):135–152
Gómez-Treviño E, Hernández FJE, Jones JMR (2014) Quadratic solution for the 2-D magnetotelluric impedance tensor distorted by 3-D electro-galvanic effects. Geophys J Int 198(3):1795–1804
Groom RW, Bailey RC (1989) Decomposition of magnetotelluric impedance tensors in the presence of local three-dimensional galvanic distortion. J Geophys Res Solid Earth 94(B2):1913–1925
Groom RW, Kurtz RD, Jones AG, Boerner DE (1993) A quantitative methodology to extract regional magnetotelluric impedances and determine the dimension of the conductivity structure. Geophys J Int 115:1095–1118
Jones A (1988) Static shift of magnetotelluric data and its removal in a sedimentary basin environment. Geophysics 53(7):967–978
Jones AG (1999) Imaging the continental upper mantle using electromagnetic methods. Lithos 48:57–80
Kelbert A, Schultz A, Egbert G (2009) Global electromagnetic induction constraints on transition-zone water content variations. Nature 460:1003–1007

Kuvshinov A, Semenov A (2012) Global 3-D imaging of mantle electrical conductivity based on inversion of observatory C-responses–I. An approach and its verification. Geophys J Int 189(3):1335–1352
Ledo J, Queralt P, Pous J (1998) Effects of galvanic distortion on magnetotelluric data over a three-dimensional regional structure. Geophys J Int 132:295–301
Lezaeta P, Haak V (2003) Beyond magnetotelluric decomposition: induction, current channeling, and magnetotelluric phases over 90. J Geophys Res Solid Earth (1978–2012) 108(B6). doi:10.1029/2001JB000990
McNeice G, Jones A (2001) Multisite, multifrequency tensor decomposition of magnetotelluric data. Geophysics 66(1):158–173
Ogawa Y, Uchida T (1996) A two-dimensional magnetotelluric inversion assuming Gaussian static shift. Geophys J Int 126(1):69–76
Oldenburg D, Ellis R (1993) Efficient inversion of magnetotelluric data in two dimensions. Phys Earth Planet Inter 81(1–4):177–200
Patro PK, Uyeshima M, Siripunvaraporn W (2013) Three-dimensional inversion of magnetotelluric phase tensor data. Geophys J Int 192(1):58–66
Pedersen LB, Engels M (2005) Routine 2D inversion of magnetotelluric data using the determinant of the impedance tensor. Geophysics 70(2):G33–G41
Rung-Arunwan T, Siripunvaraporn W, Utada H (2016) On the Berdichevsky average. Phys Earth Planet Inter 253:1–4
Sasaki Y, Meju MA (2006) Three-dimensional joint inversion for magnetotelluric resistivity and static shift distributions in complex media. J Geophys Res Solid Earth (1978–2012) 111(B5). doi:10.1029/2005JB004009
Seama N, Baba K, Utada H, Toh H, Tada N, Ichiki M, Matsuno T (2007) 1-D electrical conductivity structure beneath the Philippine Sea: results from an ocean bottom magnetotelluric survey. Phys Earth Planet Inter 162(1–2):2–12
Semenov A, Kuvshinov A (2012) Global 3-D imaging of mantle conductivity based on inversion of observatory C-responses–II. Data analysis and results. Geophys J Int 191(3):965–992
Siripunvaraporn W, Egbert G (2009) WSINV3DMT: vertical magnetic field transfer function inversion and parallel implementation. Phys Earth Planet Inter 173(3–4):317–329
Siripunvaraporn W, Egbert G, Lenbury Y, Uyeshima M (2005) Three-dimensional magnetotelluric inversion: data-space method. Phys Earth Planet Inter 150(1–3 SPEC. ISS):3–14
Smith JT (1995) Understanding telluric distortion matrices. Geophys J Int 122:219–226
Szarka L, Menvielle M (1997) Analysis of rotational invariants of the magnetotelluric impedance tensor. Geophys J Int 129(1):133–142
Tada N, Baba K, Siripunvaraporn W, Uyeshima M, Utada H (2012) Approximate treatment of seafloor topographic effects in three-dimensional marine magnetotelluric inversion. Earth Planets Space 64(11):1005–1021
Tietze K, Ritter O, Egbert GD (2015) 3-D joint inversion of the magnetotelluric phase tensor and vertical magnetic transfer functions. Geophys J Int 203(2):1128–1148
Tournerie B, Chouteau M, Marcotte D (2007) Magnetotelluric static shift: estimation and removal using the cokriging method. Geophysics 72(1):F25–F34
Utada H, Munekane H (2000) On galvanic distortion of regional three-dimensional magnetotelluric impedances. Geophys J Int 140:385–398
Watts MD, Mackie R, Scholl C, Hallinan S (2013) Limitations of MT static shift corrections using time-domain EM data. SEG Technical Program Expanded Abstracts, pp 681–684
Weaver JT, Agarwal AK, Lilley FEM (2000) Characterization of the magnetotelluric tensor in terms of its invariants. Geophys J Int 141(2):321–336
Wessel P, Smith WHF (1998) New, improved version of generic mapping tools released. Eos Trans Am Geophys Union 79(47):579–579
Wilt MJ, Williams J (1989) Layered model inversion of central-loop EM soundings near a geological contact. Explor Geophys 20(1/2):71–73